The Henryk Niewodniczański
Institute of Nuclear Physics
Polish Academy of Sciences
ul. Radzikowskiego 152, 31-342 Kraków
http://www.ifj.edu.pl/badania/publikacje

Kraków, 2023

Insight into phase situation and kinetics of cold- and melt crystallization processes of chiral smectogenic liquid crystals

Anna Drzewicz

Monograph

Wydano nakładem Instytutu Fizyki Jądrowej im. Henryka Niewodniczańskiego
Polskiej Akademii Nauk
Kraków 2023
Recenzenci: prof. Krzysztof Czupryński, prof. Maria Massalska-Arodź
ISBN: 978-83-63542-38-2 (print)
ISBN: 978-83-63542-37-5 (pdf)
https://doi.org/10.48733/978-83-63542-37-5

ABSTRACT

Liquid crystals are made up of molecules with an anisotropic shape, which means they have various properties along different directions. This makes them distinct from isotropic liquids because they tend to align themselves with specific rules and create intermediate phases called mesophases of various long-range degrees of spatial order of molecules. As they are cooled down, these partially ordered phases can either become glassy (vitrify) or form crystals. On the other hand, when liquid crystals are heated from a glassy state, they experience a phenomenon known as cold crystallization. This work discusses the studies of the phase situation and the kinetics of non-isothermal and isothermal cold- and melt crystallization of chiral smectogenic liquid crystals belonging to the 3FmX_1PhX_2r.s series. Compounds under study exhibit differences in the molecular structure, for instance in the terminal non-chiral ('m' = 2-7) and chiral ('r' = 4-7, 's' = 1, 2) chain lengths, and the fluorosubstitution of the aromatic molecular core ('X_1', 'X_2' = H, F). It is found that individual elements of the molecular structure of 3FmX_1PhX_2r.s influence to varying degrees the occurrence of liquid crystal phases or the nature of both crystallization and vitrification processes.

KEYWORDS

liquid crystals; phase transitions; glass transition; cold crystallization; molecular dynamics.

STRESZCZENIE

Ciekłe kryształy składają się z cząsteczek o anizotropowym kształcie, co oznacza, że mają odmienne właściwości w różnych kierunkach. To odróżnia je od izotropowych cieczy, ponieważ mają tendencję do porządkowania się według określonych zasad i tworzenia faz pośrednich zwanych mezofazami o różnym dalekozasięgowym stopniu uporządkowania cząsteczek. Po ochłodzeniu te częściowo uporządkowane fazy mogą ulec zeszkleniu albo utworzyć fazę krystaliczną. Z drugiej strony, gdy ciekłe kryształy są ogrzewane ze stanu szklistego, mogą ulegać zjawisku zwanym zimną krystalizacją. W pracy omówiono sytuację fazową oraz kinetykę zimnej krystalizacji i krystalizacji zachodzącej w trakcie ochładzania substancji, zarówno w warunkach nieizotermicznych jak i izotermicznych, dla chiralnych smektogennych ciekłych kryształów należących do serii 3FmX_1PhX_2r.s. Badane związki wykazują różnice w budowie molekularnej, na przykład w długościach końcowych łańcuchów niechiralnych („m" = 2-7) i chiralnych („r" = 4-7, „s" = 1, 2) oraz we fluoropodstawieniu aromatycznego rdzenia molekularnego („X_1", „X_2" = H, F). Stwierdzono, że poszczególne elementy struktury molekularnej związków 3FmX_1PhX_2r.s w różnym stopniu wpływają na występowanie faz ciekłokrystalicznych oraz na charakter procesów krystalizacji i witryfikacji.

SŁOWA KLUCZOWE

ciekłe kryształy; przejścia fazowe; przejście szkliste; zimna krystalizacja; dynamika molekularna.

ABBREVIATIONS

BDS	Broadband dielectric spectroscopy
cc	Cold crystallization
CONDIS	Conformationally disordered crystal
Cr	Crystal phase
DSC	Differential scanning calorimetry
FTIR	Fourier-transform infrared spectroscopy
gCr	Glass of crystal phase
gSmC_A*	Glass of smectic C_A* phase
gSmX_A*	Glass of smectic X_A* phase
HN	Havriliak-Negami
Iso	Isotropic phase
LC	Liquid crystal
mc	Melt crystallization
ODIC	Orientationally disordered crystal
OAFLCs	Orthoconic antiferroelectric liquid crystals
POM	Polarizing optical microscopy
SmA	Smectic A phase
SmA*	Smectic A* phase
SmC	Smectic C phase
SmC*	Smectic C* phase
SmC_α*	Smectic C_α* phase
SmC_A	Smectic C_A phase
SmC_A*	Smectic C_A* phase
SmX_A*	Smectic X_A* phase
T_{cc}	Temperature of cold crystallization
T_g	Temperature of glass transition
T_{mc}	Temperature of melt crystallization
VFT	Vogel-Fulcher-Tammann

1. Introduction

Usually, an ordered crystal melts directly into an isotropic liquid phase with randomly ordered molecules. However, for compounds with the anisotropic shape of molecules, such as rod-shaped, melting through one or more phases of various degrees of intermediate molecular ordering (called mesophases) has been observed. This is a feature of liquid crystals and Fig. 1 shows an example of the possible phase sequences of calamitic liquid crystal compounds with chiral molecules. In the smectic A (SmA) phase, the long axes of molecules are on average orthogonal to the smectic layers, while in the smectic C (SmC) phase, the molecules are tilted relative to the normal of the layers by a tilt angle. The smectic A* (SmA*) and C* (SmC*) phases are the chiral equivalents of the achiral SmA and SmC phases. As a result of the formation of the SmC* phase by chiral molecules with non-zero perpendicular component of the dipolar moments, macroscopic helical order occurs, in which the director rotates by a slight constant angle when passing from layer to layer. After unwinding a helix by the external electric field, the SmC* phase exhibits ferroelectric properties (bistable switching by an external electric field). The smectic C_A* (SmC_A*) phase differs from the SmC* phase by the anticline order of the tilt order parameter in the subsequent smectic layers. After unwinding a helix, the SmC_A* phase exhibits antiferroelectric properties (tristable switching). Both chiral phases can be used in liquid crystal display technology because devices with short switching times, large contrast and many scales can be realized [1]. Furthermore, in orthoconic antiferroelectric liquid crystals (OAFLCs) the optical axis is positioned at a right angle to the switching plane, effectively avoiding light leakage in the dark mode of a display resulting from misalignment defects in the material [2]. Smectic liquid crystals are used not only in LC displays [3], but also as the components in LC-based colloids [4] or organic electrodes [5].

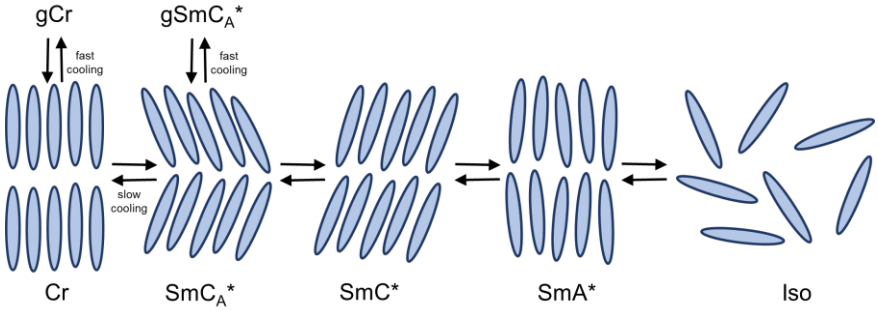

Figure 1. Possible phase sequences in liquid crystals formed by chiral molecules.

The substances forming chiral smectic phases may solidify (it is called the melt crystallization process, Fig. 2a) not only to fully ordered crystals, but they can also form orientationally (ODIC) or conformationally (CONDIS) disordered crystals. Any system that exhibits a degree of dynamic disorder can undergo vitrification, accompanied by a slowing down (or even freezing) of the stochastic molecular motions on approaching the glass transition temperature (T_g) [6]. The partially ordered glasses are formed by the ODIC [7] and CONDIS [8] crystals and SmA* [9], SmC [10], SmC* [11], SmC_A* [12] and SmI_A* [13] phases. The vitrified chiral tilted smectic phases may be used as optical filters, similarly as in case of the chiral nematics [14]. Upon heating from the glassy state, softening to supercooled liquid crystal and then the cold crystallization may be observed (Fig. 2b). This process is usually studied under isothermal and non-isothermal conditions. For some compounds, one of the two mechanisms dominates during cold crystallization: (*i*) it may proceed by classical thermodynamic predictions or (*ii*) it may occur via diffusion, associated with the mobility of molecules [12,15,16]. The compounds that form the glass during cooling and exhibit the cold crystallization after reheating are considered suitable for the energy storage [17]. Liquid crystalline compounds that do not crystallize upon cooling but stay stable in the smectic phase below the room temperature are desired components of fillings in LC displays.

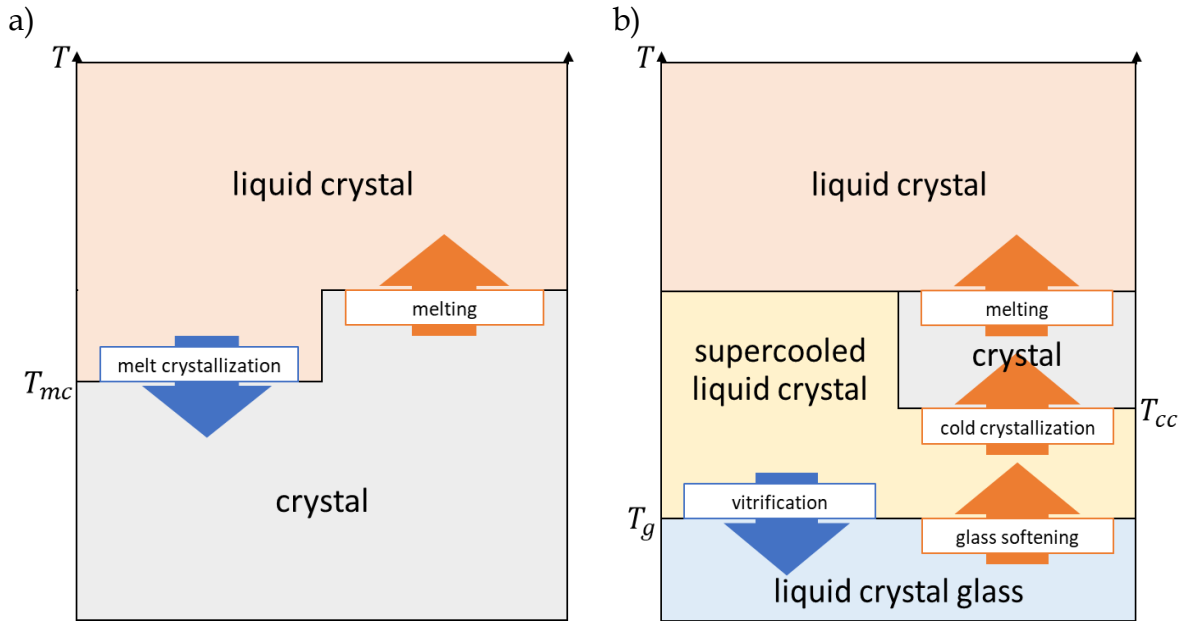

Figure 2. The scheme of melt (a) and cold (b) crystallization processes.

This paper is dedicated to the chiral smectogenic liquid crystals belonging to the series of 3FmX$_1$PhX$_2$r.s compounds (where '3F' is the C_3F_7- group, 'm' is the number of carbon atoms in the non-chiral -$(CH_2)_m$- terminal chain, 'm' = 2-7, 'X$_1$' and 'X$_2$' are hydrogen or fluorine atoms in the phenyl ring, 'X$_1$', 'X$_2$' = H, F, 'r' and 's' are the number of carbon atoms in the chiral terminal chains lengths, 'r' = 4-7, 's' = 1,2). The general formula of (*S*)-4'-(1-'s','r+1'oxycarbonyl) biphenyl-4-yl 4-['m'-(2,2,3,3,4,4,4-heptafluorobutoxy) 'm'-1-oxy]-'X$_1$','X$_2$'-fluorobenzoates is presented in Fig. 3. These homologues are systematically investigated to ascertain which features of the molecular structure play an essential role in thermodynamic processes, especially during crystallization and vitrification. The substances' phase situation is related to the interplay between molecular structure, motions and interactions between molecules. The molecular interactions dominate the physical and dynamical properties of the system and, as a result, influence the progress of the crystallization process. For instance, the dipole–dipole interactions are proven as one of the essential factors determining suppression of crystallization during cooling in various types of molecular glass formers [18]. So, this work aims to show that the phase situation and crystallization kinetics strongly depend on the molecular structure, e.g.: (*i*) the length of the terminal non-chiral ('m') and chiral ('r') chains, (*ii*) the fluorosubstitution of the aromatic molecular core ('X$_1$' and 'X$_2$'), and (*iii*) the type of the chiral centre ('r' and 's'). All compounds under study form a chiral smectic phase with antiferroelectric properties (SmC_A*) [19]. Moreover, the longest homologues ('m' = 5-7) also form a chiral smectic phase with ferroelectric properties (SmC*). The temperature range of these phases increases with the molecules length. Some compounds with the partially fluorinated phenyl ring ('X$_1$' = H, 'X$_2$' = F) undergo vitrification from the SmC_A* phase upon cooling and subsequently cold crystallization upon heating, while for the analogous fully fluorinated ('X$_1$', 'X$_2$' = F) compounds only crystallization is observed on cooling. The chiral centres based on (*S*)-(+)-3-octanol ('r.s' = 5.2) and (*S*)-(+)-2-octanol ('r.s' = 6.1) cause differences in the polymorphism of the smectic phases [20]. Some of compounds from the family of 3FmX$_1$PhX$_2$r.s fluorinated esters (such as 3F5HPhF6.1 and 3F7FPhH6.1) are suitable components of orthoconic liquid crystalline mixtures, which are characterized by the high stability of the high-tilted SmC_A* phase in the room temperature [21].

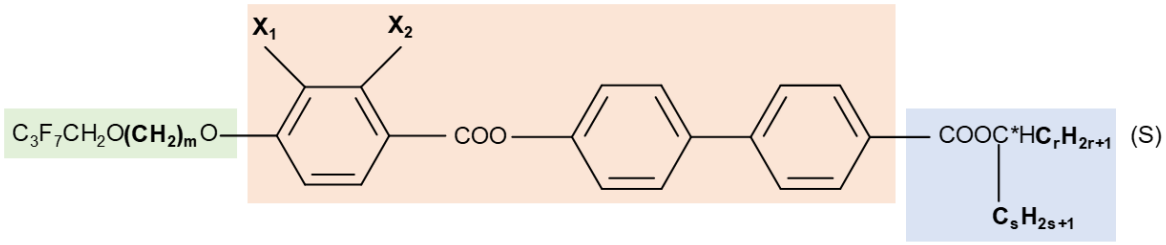

Figure 3. The chemical structure of the 3FmX$_1$PhX$_2$r.s homologues ('m' = 2-7, 'X$_1$', 'X$_2$' = H, F, 'r' = 4-7, 's' = 1,2).

In the following chapters we will discuss the influence of: (*i*) the oligomethylene spacer length of the non-chiral chain ('m' parameter), (*ii*) the fluorosubstitution of the rigid core ('X$_1$' and 'X$_2$' parameters), (*iii*) the alkyl chain length of the chiral substituent ('r' parameter), and (*iv*) the type of the chiral centre ('r' and 's' parameters) on the phase situation, crystallization/vitrification phenomena and crystallization kinetics of the 3FmX$_1$PhX$_2$r.s compounds. Our study described within this paper fits well with current research on the issues of changes in a structure and dynamics that occur in the thermodynamic phases of liquid crystals. Recently, many scientific studies have focused on liquid crystalline materials containing fluorinated molecules. When the alkyl or alkoxy chain is fluorinated, it makes the molecules more rigid and encourages the formation of smectic phases [22,23]. Additionally, replacing some hydrogens in the aromatic molecular core with fluorine affects the dielectric and electrooptic properties, and temperatures at which phase transitions occur [24,25].

This work is a summary of only a small portion of the results obtained for the 3FmX$_1$PhX$_2$r.s compounds. In the next work, the relaxation and vibrational dynamics of the investigated homologues will be discussed in greater detail. However, the remaining physicochemical properties of the 3FmX$_1$PhX$_2$r.s compounds, not mentioned in this work, are described in Refs. [26–30].

2. Experimental Details

The examined LCs were synthesized at the Institute of Chemistry, Military University of Technology, Warsaw, Poland. Details of syntheses are given in Refs.: for 3FmX$_1$PhX$_2$6.1 [19,31], for 3FmHPhH7.1 [32], for 3F5HPhH5.2 (also denoted as II.5.(HH)) [33], and for 3F5HPhF4.1 (also denoted as 3F5BFBiHex) [32].

Polarizing optical microscopy (POM) textures were observed using Leica DM2700P microscope with the crossed polarisers equipped with Linkam LNP96-S heating/cooling stage and Linkam T96-S temperature controller. The samples were placed on covered glass plates in the isotropic liquid phase and were fast cooled and subsequently slowly heated.

Differential scanning calorimetry (DSC) measurements were performed using TA DSC 2500 calorimeter. The indium and sapphire standards were used for calibration. The empty aluminium pan was used as the reference. The samples were cooled and heated with several rates (±1, ±2, ±3, ±4, ±5, ±8, ±10, ±15, ±20, ±25 and ±30) K min^{-1}.

Broadband dielectric spectra (BDS) were measured using a high-resolution Novocontrol Alpha Analyser, in the frequency range of 10^{-1} – 10^{7} Hz. The samples were placed between two gold electrodes without aligning layers with a Teflon spacer, with a thickness of ca. 50 µm. Dielectric spectra were collected according to two protocols: (*i*) upon slow cooling and heating, with the rate of 2 K min^{-1}, (*ii*) upon slow heating, with the rate of 2 K min^{-1} after fast cooling with the rate of 10 K min^{-1}. The temperature was stabilised by a Novocool temperature controller with an accuracy better than 0.1 K.

To describe the detected relaxation processes in polar materials, the complex electric permittivity $\varepsilon^*(\omega)$ is fitted in the frequency ω domain using the empirical Havriliak-Negami (HN) formula [34]:

$$\varepsilon^*(\omega) = \varepsilon_\infty + \sum_k \frac{\Delta\varepsilon_k}{\left[1+\left(i\omega\tau_{HN_k}\right)^{\alpha_{HN_k}}\right]^{\beta_{HN_k}}} + \frac{\sigma_0}{\omega\varepsilon_0}, \quad (1)$$

where ε_∞ is the electric permittivity at the high frequency limits, $\Delta\varepsilon_k$ is the dielectric strength of the k-th process, τ_{HN_k} is the dielectric relaxation time of the k-th dynamic process, σ_0 is dc electrical conductivity, ε_0 is the electric permittivity of the vacuum, and α_{HN_k} and β_{HN_k} are shape parameters describing the symmetric and asymmetric

broadening of the loss spectra, respectively. The temperature dependence of the relaxation times $\log\tau\left(\frac{1}{T}\right)$, which do not vary linearly with temperature according to the Arrhenius equation $\tau(T) = \tau_0 \exp\left(\frac{\Delta E}{RT}\right)$, ΔE means the activation energy of the molecular dynamics, can be described by the Vogel-Fulcher-Tammann (VFT) function [35]:

$$\tau_\alpha = \tau_\infty \exp\left(\frac{D_f T_0}{T - T_0}\right), \quad (2)$$

where τ_∞ is the pre-exponential factor, D_f is a constant parameter and T_0 is the Vogel temperature describing the ideal glass transition temperature.

The D_f parameter may be used to estimate the so-called fragility index m_f, described as $m_f = \left.\frac{d\log\tau_\alpha(T)}{d(T_g/T)}\right|_{T=T_g}$ using the empirical formula [36]:

$$m_f \approx 16 + \frac{590}{D_f}. \quad (3)$$

Comparison of the characteristic crystallization times τ and relaxation times τ_α of the α-process in glass forming phase shows to what extent the crystallization kinetics is controlled by diffusion, because [37]:

$$\tau \propto \tau_\alpha^{\xi}, \quad (4)$$

where ξ is the coupling coefficient. If the ξ coefficient is close to 1, the crystallization is controlled mainly by diffusion. The lower, even negative values of ξ are interpreted as crystallization controlled mostly by a thermodynamic driving force [38].

Fourier-transform infrared (FTIR) spectra were obtained using Bio-Rad Digilab FTS 3000 Excalibur FTIR spectrometer, in the wavenumber range of 4000–400 cm^{-1}, with a resolution close to 0.4 cm^{-1} and with the number of scans of 64. The samples in the form of thin films were placed between two zinc selenide ZnSe window discs. The measurements were carried out in two protocols: (*i*) upon slow cooling and heating, with the rate of 2 K min^{-1}, (*ii*) upon slow heating with the rate of 2 K min^{-1} after fast cooling with the rate of 10 K min^{-1}.

All measurements were performed under a nitrogen atmosphere, in the temperature range from 173 K to the transition temperature to the isotropic phase. For some compounds, measurements were carried out in the temperature range from 273 K to the transition temperature to the isotropic phase.

The kinetics of the non-isothermal cold crystallization was studied by the DSC method by heating the sample in the glassy state with different heating rates. The degree of crystallinity $D(T)$ of the non-isothermal cold crystallization can be calculated for each heating rate as a function of temperature, according to the formula [39]:

$$D(T) = \frac{\int_{T_b}^{T}\left(\frac{\mathrm{d}H}{\mathrm{d}T}\right)\mathrm{d}T}{\int_{T_b}^{T_e}\left(\frac{\mathrm{d}H}{\mathrm{d}T}\right)\mathrm{d}T}, \quad (5)$$

where T_b and T_e are the beginning and ending temperatures of the crystallization process, $\frac{\mathrm{d}H}{\mathrm{d}T}$ means the heat flow at a given temperature. To obtain more information about the mechanism of the cold crystallization under non-isothermal conditions, the DSC data are analysed by the Ozawa model, preferably in its logarithmic form [40]:

$$\log\big(-\ln(1 - D(T))\big) = \log(Z) - n_O \log(\mathrm{d}T/\mathrm{d}t), \quad (6)$$

where Z is the Ozawa crystallization rate and n_O is the Ozawa exponent depending on the crystal size.

The activation energy of the cold crystallization process under non-isothermal conditions may be determined based on two methods: the Kissinger equation [41] connects the activation energy (E_A) of crystallization with the heating rate ($\mathrm{d}T/\mathrm{d}t$) and the temperature (T_m) corresponding to the maximum of the exothermic anomaly in the DSC thermogram via the formula:

$$\ln\left(\frac{\mathrm{d}T/\mathrm{d}t}{T_m^2}\right) = -\frac{E_A}{RT_m} + const, \quad (7)$$

while the Augis-Bennett equation [42] includes additionally the initial cold crystallization temperature (T_i):

$$\ln\left(\frac{\mathrm{d}T/\mathrm{d}t}{T_m - T_i}\right) = -\frac{E_A}{RT_m} + const. \quad (8)$$

The kinetics of the isothermal cold crystallization was determined by the selected experimental method according to the following protocol: (*i*) the samples were fast cooled from the isotropic phase to 173 K, and subsequently slowly heated to the chosen cold crystallization temperatures (T_{cc}); (*ii*) the samples were kept at T_{cc} temperature until full cold crystallization was completed.

The kinetics of the melt crystallization under isothermal conditions was investigated by the selected experimental method according to the following protocol: (*i*) the samples were slowly cooled from the isotropic phase to the chosen melt

crystallization temperatures (T_{mc}); (ii) the samples were kept at T_{mc} temperature until full melt crystallization was completed.

The degree of crystallinity $D(t)$ of the isothermal crystallization can be calculated from the formulas:

$$D(t) = \frac{\int_{t_b}^{t}\left(\frac{\mathrm{d}H}{\mathrm{d}t}\right)\mathrm{d}t}{\int_{t_b}^{t_e}\left(\frac{\mathrm{d}H}{\mathrm{d}t}\right)\mathrm{d}t}, \quad (9)$$

for DSC results, where t_b and t_e are the beginning and end time of crystallization [43];

$$D(t) = \Delta\varepsilon_N(t) = \frac{\Delta\varepsilon(0)-\Delta\varepsilon(t)}{\Delta\varepsilon(0)-\Delta\varepsilon(\infty)}, \quad (10)$$

for BDS results, where the crystallization degree $D(t)$ is replaced by the normalized dielectric strength $\Delta\varepsilon_N(t)$, and $\Delta\varepsilon(0)$, $\Delta\varepsilon(t)$ and $\Delta\varepsilon(\infty)$ are the dielectric increment at the beginning, at the chosen time and at the end of the observations, respectively [44];

$$D(t) = I(t) = \frac{I_t-I_e}{I_o-I_e}, \quad (11)$$

for FTIR results, where the crystallization degree $D(t)$ is replaced by the normalized carbonyl bands intensities $I(t)$, and I_o, I_t and I_e are the initial, at some time t and the final band intensities during isothermal process. Knowledge of the isothermal crystallization degree allows to describe the kinetics of this process using the Avrami model, here in its logarithmic form [45]:

$$\ln(-\ln(1-D(t))) = \ln k + n_A \ln(t-t_o), \quad (12)$$

where n_A is the Avrami exponent and its value depends on the nucleation rate and dimensionality of the crystal growth, and k depends on nucleation and crystal growth rate.

3. Influence of the oligomethylene spacer ('m' parameter)

3.1. 3FmX$_1$PhX$_2$6.1 compounds ('m' = 2-7, 'X$_1$' = H, F, 'X$_2$' = H, F)

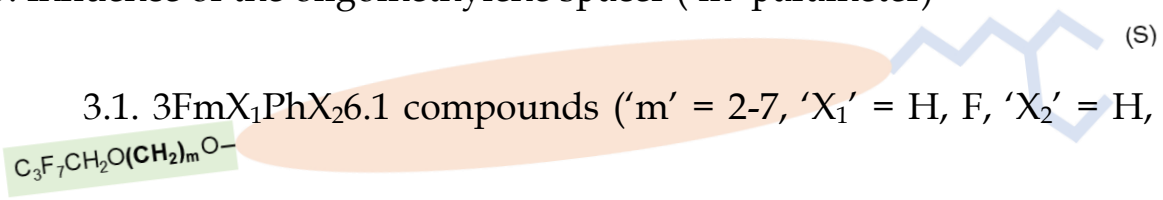

In this chapter, we compare 3FmHPhH6.1, 3FmHPhF6.1, 3FmFPhH6.1 and 3FmFPhF6.1 compounds, which differ in the length of the oligomethylene -(CH$_2$)$_m$- spacer in the non-chiral chain ('m' = 2-7). In general, the phase transitions of shorter homologues with 'm' = 2-4 are determined upon DSC measurements carried out upon slow cooling and/or heating with the rate of 2-3 K min^{-1} in the temperature range from 273 K to the transition temperature to the isotropic phase. Presumably, this is a reason why we do not observe any glass transition for these samples. The comparison of the phase situations for cooling/heating of all discussed compounds is shown in Fig. 4 (for 3FmHPhH6.1), Fig. 5 (for 3FmHPhF6.1), Fig. 6 (for 3FmFPhH6.1) and Fig. 7 (for 3FmFPhF6.1). The exact values of the phase transition temperatures are given in Tab. 5.

All compounds with 'm' = 2 exhibit the same two smectic phases and one crystal phases upon slow heating: (*i*) Cr (342 K) SmC$_A$* (388 K) SmC* (401 K) Iso for 3F2HPhH6.1, (*ii*) Cr1 (326 K) SmC$_A$* (368 K) SmC* (375 K) Iso for 3F2HPhF6.1, (*iii*) Cr (343 K) SmC$_A$* (373 K) SmC* (384 K) Iso for 3F2FPhH6.1, (*iv*) Cr (332 K) SmC$_A$* (375 K) SmC* (386 K) Iso for 3F2FPhF6.1. For 3F2HPhF6.1, the second crystal phase is observed only for fast cooling: Iso (377 K) SmC* (364 K) SmC$_A$* (307 K) Cr1 (299 K) Cr2, and heating: Cr2 (321 K) Cr1 (326 K) SmC$_A$* (368 K) SmC* (375 K) Iso, with the rates of 6 K min^{-1} and higher.

Increasing the molecule length by one (-CH$_2$-) group affects the change in the smectic polymorphism. All samples with 'm' = 3 possess only the SmC$_A$* phase upon slow heating: (*i*) Cr (352 K) SmC$_A$* (389 K) Iso for 3F3HPhH6.1, (*ii*) Cr (306 K) SmC$_A$* (362 K) Iso for 3F3HPhF6.1, (*iii*) Cr (324 K) SmC$_A$* (372 K) Iso for 3F3FPhH6.1, (*iv*) Cr (347 K) SmC$_A$* (370 K) Iso for 3F3FPhF6.1. However, the shape of the DSC thermograms of 3F3HPhF6.1 in Ref. [46] indicates only partial crystallization during heating. It suggests that this compound may form the glass of the SmC$_A$* phase in lower temperatures.

The polymorphism of smectic and crystal phases for compounds with 'm' = 4 is more diversified. Upon slow heating, the phase situation of 3F4HPhH6.1 is: Cr2 (329 K) Cr1/SmC_A* (346 K) SmC_A* (381 K) SmC* (403 K) Iso. In comparison, upon slow cooling there is also the SmX_A* phase: Iso (403 K) SmC* (378 K) SmC_A* (301 K) SmX_A* (299 K) Cr2. The hexatic SmX_A* phase can be either SmI_A* or SmF_A*. These tilted phases differ from the SmC_A* phase by developing of the bond orientation order within the smectic layers [47]. The 3F4HPhF6.1 compound forms more crystal phases upon slow heating: Cr2 (312 K) Cr1 (319 K) SmC_A* (359 K) SmC* (379 K) Iso, than upon slow cooling: Iso (380 K) SmC* (356 K) SmC_A* (282 K) Cr2. For 3F4FPhH6.1, we observe three smectic phases upon slow heating: Cr (346 K) SmC_A* (369 K) SmC* (386 K) SmA* (388 K) Iso. The 3F4FPhF6.1 compound exhibits a richer crystal phase polymorphism upon slow heating: Cr3 (346 K) Cr2 (348 K) Cr1 (355 K) SmC_A* (368 K) SmC* (388 K) Iso, than upon slow cooling: Iso (389 K) SmC* (366 K) SmC_A* (333 K) Cr3.

All samples with 'm' = 5 vitrify during cooling and during subsequent heating the cold crystallization process is observed. For 3F5HPhH6.1, the glass transition occurs from the SmX_A* phase upon fast cooling with the rates of 5-20 K min^{-1}: Iso (397 K) SmC* (393 K) SmC_A* (283 K) SmX_A* (T_g = 247 K) $gSmX_A$*, while slow cooling with the rate of 2 K min^{-1} leads to its crystallization: SmX_A* (T_{mc} = 276 K) Cr2. The phase situation upon fast heating is as follows: $gSmX_A$* (~225 K) SmX_A* (T_{cc} = 275 K) Cr2 (306 K) Cr1 (335 K) SmC_A* (395 K) SmC* (397 K) Iso, while upon slow heating, we observe Cr2 (293 K) Cr1 phase transition at a lower temperature. The 3F5HPhF6.1 vitrifies from the SmC_A* phase even upon slow cooling with the rate of 2 K min^{-1}: Iso (371 K) SmA* (370 K) SmC* (368 K) SmC_A* (T_g = 230 K) $gSmC_A$*. Upon subsequent heating, there is a rich polymorphism of crystal phases: $gSmC_A$* (~230 K) SmC_A* (T_{cc} = 253 K) Cr3 (278 K) Cr2 (290 K) Cr1/Cr2 (301 K) SmC_A* (369 K) SmC* (370 K) SmA* (372 K) Iso. For 3F5FPhH6.1, the vitrification occurs from the Cr2 phase even upon slow cooling with the rate of 2 K min^{-1}: Iso (383 K) SmA* (380 K) SmC* (379 K) SmC_A* (297 K) Cr2 (T_g = 253 K) gCr2. The phase behaviour upon subsequent heating is: gCr2 (~236 K) Cr2 (T_{cc} = 306 K) Cr1 (343 K) SmC_A* (380 K) SmC* (380 K) SmA* (383 K) Iso. The 3F5FPhF6.1 also vitrifies from the SmC_A* phase upon fast cooling with the rates of 5-30 K min^{-1}: Iso (383 K) SmA* (381 K) SmC_α* (381 K) SmC* (379 K) SmC_A* (T_g = 233-238 K) $gSmC_A$*, while slow cooling with the rate of 2 K min^{-1} leads to its

crystallization at T_{mc} = 296 K. Upon heating after fast cooling, the phase transitions are as follows: gSmC$_A$* (~241 K) SmC$_A$* (T_{cc} = 258 K) Cr2 (293 K) Cr1 (324 K) SmC$_A$* (380 K) SmC* (381 K) SmC$_\alpha$* (381 K) SmA* (382 K) Iso.

The feature of compounds with 'm' = 6 is the formation of the same three smectic phases, SmC$_A$*, SmC* and SmA* phases. The 3F6HPhH6.1 crystallises upon cooling with the rate of 2 K min^{-1}: Iso (400 K) SmA* (398 K) SmC* (362 K) SmC$_A$* (T_{mc} = 285 K) Cr, and upon subsequent heating, the phase situation is as follows: Cr (333 K) SmC$_A$* (368 K) SmC* (398 K) SmA* (400 K) Iso. For 3F6HPhF.1, the glass transition from the SmC$_A$* phase occurs even on slow cooling with the rate of 2 K min^{-1}: Iso (380 K) SmA* (379 K) SmC* (342 K) SmC$_A$* (T_g = 231 K) gSmC$_A$*. Upon subsequent heating, additionally two crystal phases appear: gSmC$_A$* (~230 K) SmC$_A$* (T_{cc} = 288 K) Cr2 (294 K) Cr1 (314 K) SmC$_A$* (348 K) SmC* (379 K) SmA* (380 K) Iso. On the other hand, 3F6FPhH6.1 does not vitrify even during fast cooling: Iso (386 K) SmA* (382 K) SmC* (346 K) SmC$_A$* (T_{mc} = 304 K) Cr2. Upon subsequent heating, the phase behaviour is: Cr2 (276 K) Cr1 (331 K) SmC$_A$* (355 K) SmC* (382 K) SmA* (387 K) Iso. For 3F6FPhF6.1, there is a lack of glass transition. The phase behaviour upon heating with the rate of 2 K min^{-1} is as follows: Cr (336 K) SmC$_A$* (358 K) SmC* (384 K) SmA* (386 K) Iso.

Similarly, for samples with 'm' = 7, as for their homologues with 'm' = 5, there are the glass transition and cold crystallization processes for all compounds. For 3F7HPhH6.1, the vitrification of the SmX$_A$* is observed for cooling rates of 5-20 K min^{-1}: Iso (397 K) SmA* (394 K) SmC* (388 K) SmC$_A$* (263 K) SmX$_A$* (T_g = 230 K) gSmX$_A$*, although for 2-5 K min^{-1} also partial crystallization of the sample occurs: SmC$_A$* (263 K) Cr2/SmX$_A$* (230 K) Cr2/gSmX$_A$*. The phase situation upon heating is as follows: gSmX$_A$* (~233 K) SmX$_A$* (T_{cc} = 252 K) Cr2 (275 K) Cr1 (330 K) SmC$_A$* (390 K) SmC* (394 K) SmA* (396 K) Iso. The 3F7HPhF6.1 vitrifies from the SmC$_A$* phase upon cooling with the rate of 6 K min^{-1}: Iso (374 K) SmA* (372 K) SmC* (366 K) SmC$_A$* (T_g = 221 K) gSmC$_A$*, and upon subsequent heating: gSmC$_A$* (~221 K) SmC$_A$* (T_{cc} = 242 K) Cr (298 K) SmC$_A$* (368 K) SmC* (372 K) SmA* (374 K) Iso. The polymorphism of 3F7FPhH6.1 strongly depends on the thermal treatment. Upon fast cooling with the rates of 5-20 K min^{-1}, only smectic phases are formed: Iso (377 K) SmA* (376 K) SmC* (369 K) SmC$_A$* (T_g = 233 K) gSmC$_A$*, and an analogous situation occurs

upon fast heating: gSmC$_A$* (~233 K) SmC$_A$* (371 K) SmC* (372 K) SmA* (377 K) Iso. However, upon slow cooling with the rate of 2 K min^{-1}, additionally the SmC$_\alpha$* (371 K) SmC* phase transition appears, and upon subsequent heating, the phase behaviour is: gSmC$_A$* (~233 K) SmC$_A$* (T_{cc} = 280 K) Cr2 (292 K) Cr1 (304 K) SmC$_A$* (371 K) SmC* (372 K) SmC$_\alpha$* (372 K) SmA* (377 K) Iso. For 3F7FPhF6.1, the glass transition from the Cr2 phase occurs upon cooling with the rates of 2-20 K min^{-1}: Iso (382 K) SmA* (379 K) SmC* (377 K) SmC$_A$* (301 K) Cr2 (T_g = 213 K) gCr2, and upon subsequent heating: gCr2 (~223 K) Cr2 (320 K) Cr1 (322 K) SmC$_A$* (378 K) SmC* (379 K) SmA* (382 K) Iso.

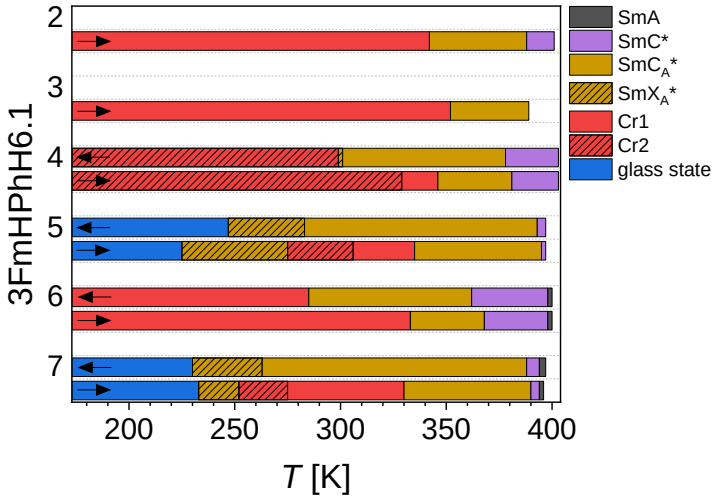

Figure 4. Phase transitions of the 3FmHPhH6.1 compounds during cooling and heating.
The transition temperatures of 3F2HPhH6.1 are taken from Ref. [19], of 3F3HPhH6.1 from Ref. [19], of 3F4HPhH6.1 from Ref. [48], of 3F5HPhH6.1 from Ref. [49], of 3F6HPhH6.1 from Ref. [50] and of 3F7HPhH6.1 from Ref. [51].

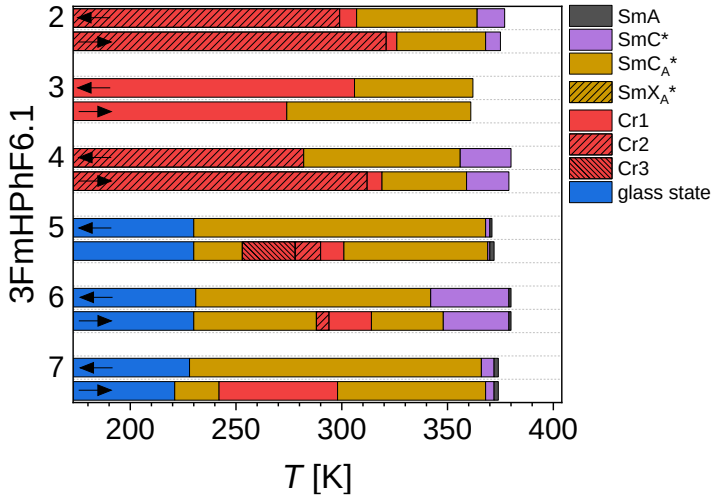

Figure 5. Phase transitions of the 3FmHPhF6.1 compounds during cooling and heating.
The transition temperatures of 3F2HPhF6.1 are taken from Ref. [52], of 3F3HPhF6.1 from Ref. [46], of 3F4HPhF6.1 from Ref. [52], of 3F5HPhF6.1 from Refs. [29,52,53], of 3F6HPhF6.1 from Refs. [29,52,53] and of 3F7HPhF6.1 from Refs. [54–56].

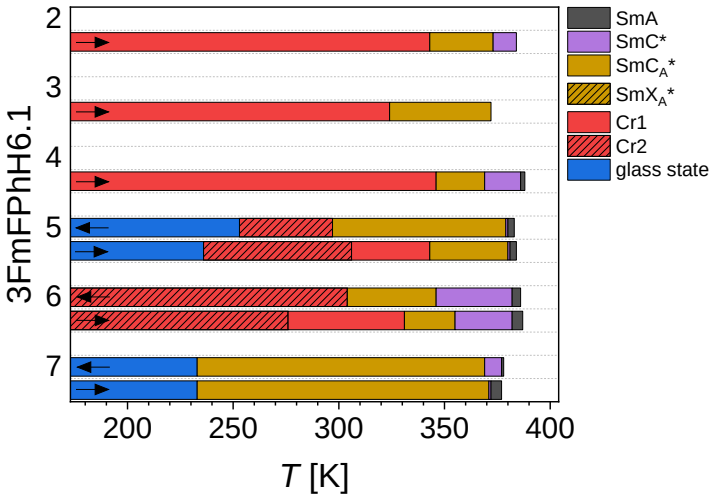

Figure 6. Phase transitions of the 3FmFPhH6.1 compounds during cooling and heating.
The transition temperatures of 3F2FPhH6.1 are taken from Ref. [19], of 3F3FPhH6.1 from Ref. [19], of 3F4FPhH6.1 from Ref. [19], of 3F5FPhH6.1 from Ref. [57], of 3F6FPhH6.1 from Ref. [50] and of 3F7FPhH6.1 from Ref. [58].

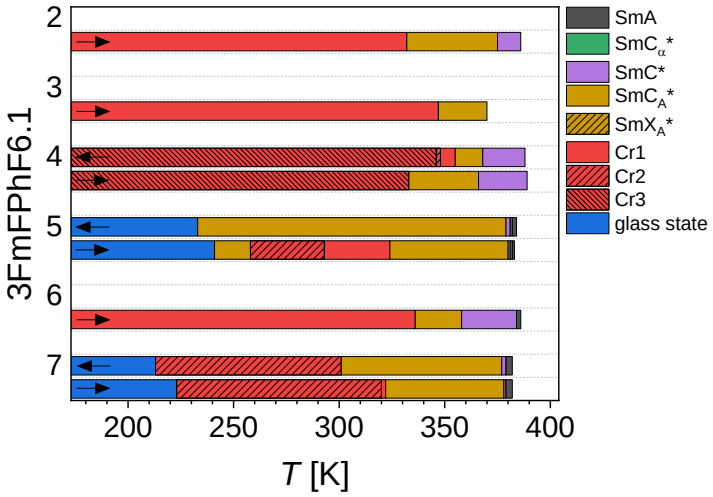

Figure 7. Phase transitions of the 3FmFPhF6.1 compounds during cooling and heating.
The transition temperatures of 3F2FPhF6.1 are taken from Ref. [19], of 3F3FPhF6.1 from Ref. [19], of 3F4FPhF6.1 from Ref. [48], of 3F5FPhF6.1 from Refs. [29,59,60], of 3F6FPhF6.1 from Ref. [29] and of 3F7FPhF6.1 from Refs. [56,61].

The details of cold- and melt crystallization, as well as the glass transition of the 3FmX$_1$PhX$_2$6.1 homologues ('m' = 5-7; 'X$_1$' = H, F; 'X$_2$' = H, F) are presented in Tab. 1. The cold crystallization under non-isothermal conditions is investigated using DSC measurements according to the Ozawa model (Eq. 6). For 3F5HPhH6.1, this process occurs with a two-dimensional crystal growth according to POM observations (with average value of n_O = 3.1) and it depends on the diffusion at lower temperatures and for higher temperatures the diffusion and thermodynamic mechanisms have comparable impact on the crystallization process [49]. The value of the coupling coefficient of 3F5HPhH6.1 (Fig. 7), calculated based on Eq. 4, means a mainly diffusion-

controlled cold crystallization, which is in accordance with the Ozawa model. According to the Kissinger (Eq. 7) and Augis-Bennett (Eq. 8) models, for 3F5HPhH6.1 there are two regimes of cold crystallization described by E_A = 141 kJ mol^{-1} for heating rates of 1-5 K min^{-1} and E_A = 73 kJ mol^{-1} for heating rates of 8-20 K min^{-1} [49]. For 3F5FPhF6.1, the non-isothermal cold crystallization rate occurs with three-dimensional crystal growth according to POM observations (n_O = 2.6-3.4) and is dependent mainly on diffusion at lower temperatures, while for higher temperatures the diffusion and thermodynamic mechanisms have a comparable influence on the crystallization kinetics. The activation energy for slow heating (E_A = 95 kJ mol^{-1}) is more significant than for fast heating (E_A = 64 kJ mol^{-1}) [60].

The isothermal cold crystallization is investigated using DSC and BDS methods and described by the Avrami model (Eq. 12). For 3F7HPhH6.1, the diffusion has a decisive role in this process occurring with three-dimensional crystal growth according to POM observations (n_A = 2.8-3.0) and with the activation energy of 114 kJ mol^{-1} [51]. A strong coupling coefficient confirms the significant influence of diffusion, as it equals 0.80 (Fig. 8). For 3F5HPhF6.1, the thermodynamic mechanism influences the crystallization kinetics more than for 3F6HPhF6.1, although diffusion still has a more prominent role for both homologues. The isothermal cold crystallization occurs with faster growth in two dimensions according to POM observations for 'm' = 6 (n_A = 2.6-2.9), with E_A = 106 kJ mol^{-1} and ζ = 0.64 (Fig. 8), while for 'm' = 5 this is one-dimensional growth of needle-like crystallites according to POM observations (n_A = 1.2), with E_A = 48 kJ mol^{-1} and ζ = 0.26 (Fig. 8) [53]. For 3F7HPhF6.1, we observe the diffusive mechanisms of both isothermal (n_A = 2.7-3.1) and non-isothermal (n_O = 4.9) three-dimensional cold crystallization. The activation energy of the isothermal process (E_A = 79 kJ mol^{-1}) is twice as large as the activation energy of the non-isothermal one (E_A = 34 kJ mol^{-1}) [54,55]. For 3F7FPhH6.1, the cold crystallization under isothermal conditions is not a simple diffusion-controlled process because of the presence of two crystal phases which can co-nucleate. Moreover, nucleation occurs not only at the beginning of the crystallization, but also simultaneously with the crystal growth and reducing dimensionality of growing crystals at lower temperatures (n_A = 0.9-3.4, E_A = 35 kJ mol^{-1}) [58,62]. For 3F5FPhF6.1, the isothermal cold crystallization depends mainly on diffusion rate with increasing dimensionality of crystal growth

from plate-like crystallites to isotropic ones according to POM observations (n_A = 2.0-3.2, E_A = 76 kJ mol^{-1}) [60].

The melt crystallization under isothermal conditions is studied by DSC and POM methods, using the Avrami model (Eq. 12). For 3F5HPhH6.1, the isothermal melt crystallization is a thermodynamic-controlled process with two-dimensional crystal growth according to POM observations (n_A = 2.7-2.9) [49]. For 3F7HPhH6.1, the kinetics of this process is controlled mainly by the rate of diffusion of molecules, with the same activation energy as for isothermal cold crystallization and different dimensional crystal growth for low temperatures (three-dimensional, n_A = 3.6) and high temperatures (two-dimensional, n_A = 2.5-2.9) [51]. For 3F6HPhF6.1, this process occurs with the two-dimensional growth of crystals with a discoidal shape according to POM observations (n_A = 2.7) and with a very low nucleation rate (only three crystallites are formed during crystallization per 1.5 hour) [53]. For 3F5FPhH6.1, melt crystallization shows different mechanisms depending on temperature, which is explained by the relation between the thermodynamic driving force and the diffusion mechanism [57]. For 3F5FPhF6.1, the melt crystallization is restricted by slow nucleation with two-dimensional crystal growth according to POM observations (n_A = 2.3-3.4, E_A = 343 kJ mol^{-1}) [60]. For 3F7FPhF6.1, this process is controlled mainly by thermodynamic and occurs with the two-dimensional growth of plate-like crystallites according to POM observations with a constant nucleation rate (n_A = 2.8-3.1). The energy barrier for nucleation equals 205 kJ mol^{-1} [56].

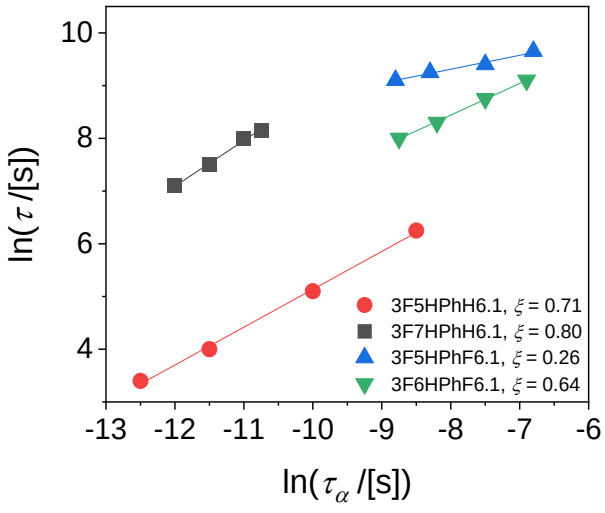

Figure 8. Coupling between the crystallization time and the α-relaxation time of the 3FmX$_1$PhX$_2$6.1. The data results of 3F5HPhH6.1 are taken from Ref. [49], of 3F7HPhH6.1 from Ref. [51], of 3F5HPhF6.1 from Ref. [53], of 3F6HPhF6.1 from Ref. [53].

The BDS spectra are obtained after fast cooling to avoid melt crystallization and thus enable the investigation of the α-relaxation process in the glass forming phase. This process is described by the HN model (Eq. 1), and the α-relaxation times are fitted with one set of the VFT formula (Eq. 2). The T_g values are defined as $\tau_\alpha(T_g)$ = 100 s [63], and the m_f parameters are determined according to Eq. 3. For 3F5HPhH6.1, T_g = 237 K and m_f = 89 (therefore this compound has an average fragility) [49]. For 3F7HPhH6.1, T_g = 229 K and m_f = 95 (high fragility parameter indicates that this sample should easily undergo cold crystallization after heating above the glass softening temperature) [51]. For 3F5HPhF6.1, T_g = 230 K and m_f = 107, while for 3F6HPhF6.1, T_g = 232 K and m_f = 129. The fragility index has a greater value for 'm' = 6 than for 'm' = 5, while the coupling coefficient is much smaller for 'm' = 5 than for 'm' = 6 [53]. The ζ parameter usually increases with decreasing of m_f according to the formula: $\zeta \approx 1.1 - 0.005 m_f$ [37]. However, this formula is based on isotropic glass formers, while both 3FmHPhF6.1 ('m' = 5, 6) homologues form the glass of the SmC_A^* phase, which is anisotropic and possesses partial positional ordering. Similar fragility index (m_f = 102) and lower glass transition temperature (T_g = 223 K) are obtained for 3F7HPhF6.1 [54,55]. The m_f = 72 value classifies 3F7FPhH6.1 as a glass former below T_g = 231 K with intermediate fragility [58,62]. The 3F5FPhF6.1 is a fragile glass former, as its m_f = 105 and T_g = 238 K [60].

The fragility index values for the $3FmX_1PhX_26.1$ compounds are in the 72-129 range. This suggests that the fragility does not depend on whether the vitrification occurs in the SmC_A^* or SmX_A^* phase.

Table 1. Parameters of cold- and melt crystallization as well as glass transition of the 3FmHPhH6.1, 3FmHPhF6.1, 3FmFPhH6.1 and 3FmFPhF6.1 compounds ('m' = 5-7). The data results of 3F5HPhH6.1 are taken from Ref. [49], of 3F7HPhH6.1 from Ref. [51], of 3F5HPhF6.1 from Ref. [53], of 3F6HPhF6.1 from Ref. [53], of 3F7HPhF6.1 from Refs. [54,55], of 3F5FPhH6.1 from Ref. [57], of 3F7FPhH6.1 from Refs. [58,62], of 3F5FPhF6.1 from Ref. [60] and of 3F7FPhF6.1 from Ref. [56] .

3FmHPhH6.1	Non-isothermal cc	Isothermal cc	Isothermal mc	Glass transition
'm' = 5	n_O = 3.1 E_A = 73-141 kJ mol^{-1} mechanism: diffusion (low T), diffusion + thermodynamic (high T)		n_A = 2.7-2.9 mechanism: thermodynamic	from SmX_A* T_g = 237 K m_f = 89
'm' = 7		n_A = 2.8-3.0 E_A = 114 kJ mol^{-1} mechanism: diffusion	n_A = 3.6 (low T) n_A = 2.5-2.9 (high T) E_A = 114 kJ mol^{-1} mechanism: diffusion	from SmX_A* T_g = 229 K m_f = 95
3FmHPhF6.1	Non-isothermal cc	Isothermal cc	Isothermal mc	Glass transition
'm' = 5		n_A = 1.2 E_A = 48 kJ mol^{-1} mechanism: diffusion		from SmC_A* T_g = 230 K m_f = 107
'm' = 6		n_A = 2.6-2.9 E_A = 106 kJ mol^{-1} mechanism: diffusion	n_A = 2.7	from SmC_A* T_g = 232 K m_f = 129
'm' = 7	n_O = 4.9 E_A = 34 kJ mol^{-1} mechanism: diffusion	n_A = 2.7-3.1 E_A = 79 kJ mol^{-1} mechanism: diffusion		from SmC_A* T_g = 223 K m_f = 102
3FmFPhH6.1	Non-isothermal cc	Isothermal cc	Isothermal mc	Glass transition
'm' = 5			n_A = 2.2-4.4 mechanism: complex	from Cr2
'm' = 7		n_A = 0.9-3.4 E_A = 35 kJ mol^{-1} mechanism: thermodynamic + diffusion		from SmC_A* T_g = 231 K m_f = 72
3FmFPhF6.1	Non-isothermal cc	Isothermal cc	Isothermal mc	Glass transition
'm' = 5	n_A = 2.6-3.4 E_A = 64-95 kJ mol^{-1} mechanism: diffusion (low T), diffusion + thermodynamic (high T)	n_A = 2.0-3.2 E_A = 76 kJ mol^{-1} mechanism: diffusion	n_A = 2.3-3.4 E_A = 343 kJ mol^{-1} mechanism: thermodynamic	from SmC_A* T_g = 238 K m_f = 105
'm' = 7			n_A = 2.8-3.1 E_A = 205 kJ mol^{-1} mechanism: thermodynamic	from Cr2

The length of the oligomethylene -$(CH_2)_m$- chain influences the polymorphism of the smectic phases and the crystallization process. In the family of the 3FmHPhF6.1 compounds, for the homologues with 'm' = 5-7, glass transition of the SmC_A* phase upon cooling and cold crystallization upon subsequent heating are observed [52,54,55]. This behaviour is not observed for the homologues with a shorter carbon chain ('m' = 2-4) [52]. For 3F4HPhF6.1, a competition between crystallisation and vitrification is pronounced. For 3F2HPhF6.1, the vitrification of the SmC_A* phase is not seen even for cooling with rates up to 20 K min^{-1}. In the remaining series, only homologues with 'm' = 5 and 7 vitrify, however there is no correlation between the length of the non-chiral chain and the type of a phase that undergoes glass transition. Both 3F5HPhH6.1 and 3F7HPhH6.1 compounds vitrify from the SmX_A* phase. The 3F5FPhH6.1 crystallizes even upon fast cooling and the melt crystallization is a complex process [57]. The 3F7FPhH6.1 is a glass former undergoing the vitrification of the SmC_A* phase, even for the lowest applied cooling rate [58,62]. Only for this compound, thermodynamic and diffusion have a comparable impact on the isothermal cold crystallization kinetics. The 3F6FPhF6.1 compound crystallizes at relatively small undercooling [64], while the 3F5FPhF6.1 compound shows intermediate properties, as its crystallization occurs slowly and can be avoided for cooling rates higher than 10 K min^{-1} [59,65]. On the other hand, 3F7FPhF6.1 crystallizes upon cooling with the 20 K min^{-1} rate [61]. It may be concluded that the glass of the smectic phase is more often observed for the odd $3FmX_1PhX_2$6.1 homologues [49,50,53,54].

3.2. 3FmHPhH7.1 compounds ('m' = 3, 5, 7)

$C_3F_7CH_2O(CH_2)_mO-$

The 3FmHPhH7.1 compounds also differ in the oligomethylene chain length ('m' = 3, 5 or 7) and have a longer chiral chain than those of the 3FmHPhH6.1 series. According to DSC results, 3F3HPhH7.1 vitrifies from the Cr phase upon fast cooling with the rates of 5-30 K min^{-1}: Iso (383 K) SmC$_A$* (309 K) Cr (T_g = 247 K) gCr, and upon subsequent heating the phase situation is similar: gCr (308 K) Cr (357 K) SmC$_A$* (383 K) Iso (Fig. 9). Upon slow cooling with the rate of 2 K min^{-1}, this compound crystallizes below T_{mc} = 320 K without vitrification.

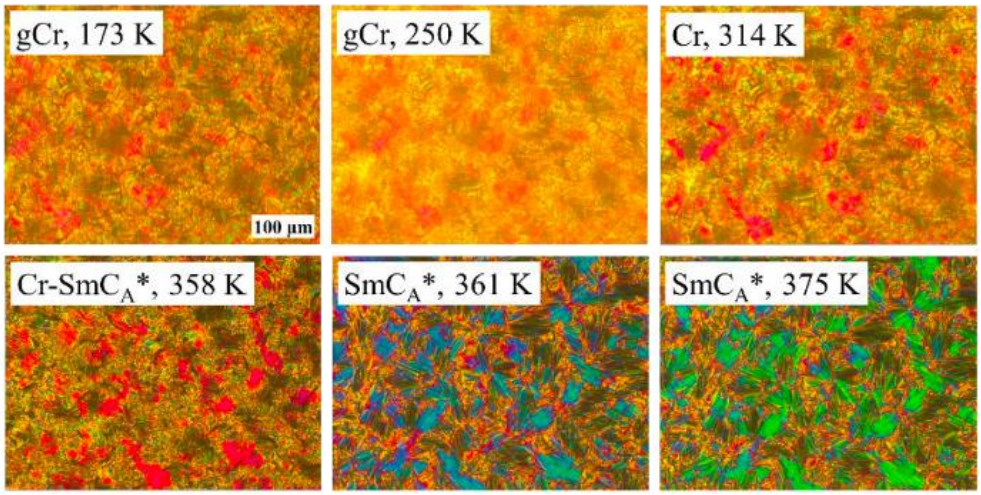

Figure 9. POM textures of 3F3HPhH7.1. Adapted with permission from [66] (according to an open access Creative Commons CC BY license).

The phase behaviour of 3F5HPhH7.1 upon fast cooling with the rates of 3-30 K min^{-1} is as follows: Iso (389 K) SmC* (380 K) SmC$_A$* (275 K) SmX$_A$* (T_g = 244 K) gSmX$_A$*, while slow cooling with the rates of 1-2 K min^{-1} leads to the melt crystallization at T_{mc} = 270 K. Upon heating after fast cooling, additionally the cold crystallization and the melting of two crystal phases are observed: gSmX$_A$* (~240 K) SmX$_A$* (T_{cc} = 265 K) Cr2 (305 K) Cr1 (335 K) SmC$_A$* (380 K) SmC* (389 K) Iso. The 3F7HPhH7.1 sample vitrifies from the SmC$_A$* phase upon fast cooling with the rates of 2-30 K min^{-1}: Iso (390 K) SmA* (388 K) SmC* (374 K) SmC$_A$* ($T_{g,1}$ = 259 K) gSmC$_A$*. Additionally, BDS measurements reveal the existence of the second glass transition at $T_{g,2}$ = 239 K (Fig. 10a). The melt crystallization upon slow cooling with the rate of 1 K min^{-1} is observed at T_{mc} = 286 K. The phase situation upon heating after fast cooling

is as follows: gSmC$_A$* (~260 K) SmC$_A$* (T_{cc} = 269 K) Cr (331 K) SmC$_A$* (380 K) SmC* (389 K) SmA* (390 K) Iso. Additionally, for 3F7HPhH7.1, the influence of external pressure on the phase situation has been shown [67]. Considering the resulting measurement uncertainty, it can be seen the linear relationships between the crystallization temperature and the pressure (grey line in Fig. 10b) as well as between the equilibrium state of the SmC$_A$* phase and the non-equilibrium state (red line in Fig. 10b). The application of pressure can induce a displacement of molecules in alignment with their preferred orientation in the liquid-like smectic phases and thus, can cause a change of the layer structure [68].

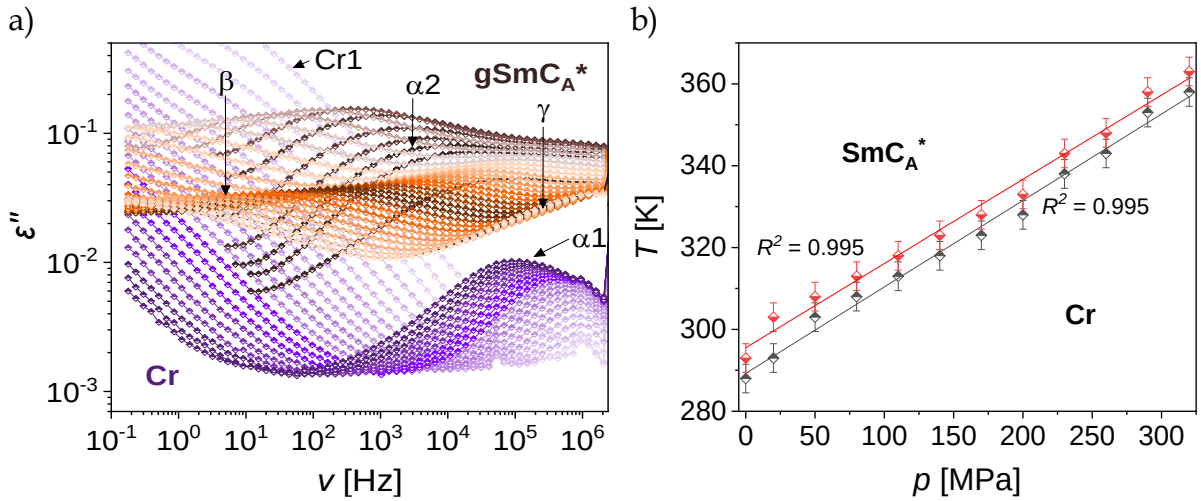

Figure 10. The BDS spectra obtained upon heating after fast cooling of the sample [69] (a) and pressure dependence of the crystallization temperature determined from BDS measurements under isobaric conditions [67] (b) of 3F7HPhH7.1. Reproduced from Refs. [67,69] with permission from the Royal Society of Chemistry.

The comparison of the phase situations for fast cooling/heating rates of all 3FmHPhH7.1 compounds is shown in Fig. 11. The exact values of the phase transition temperatures are given in Tab 5. As the 'm' parameter increases, a given LC possess a more significant number of mesophases: (*i*) the SmC$_A$* phase for 'm' = 3, (*ii*) the SmC*, SmC$_A$* and monotropic SmX$_A$* phases for 'm' = 5, (*iii*) the SmA*, SmC* and SmC$_A$* phases for 'm' = 7. The temperature range of the SmC$_A$* occurrence and the temperature of the LC-isotropic phase transition increase with the length of the molecule. All isomers vitrify upon fast cooling, however the 'm' parameter affects the glass transition behaviour: (*i*) vitrification from the CONDIS crystal phase for 'm' = 3, (*ii*) glass transition from the monotropic SmX$_A$* phase for 'm' = 5, (*iii*) vitrification from the less ordered SmC$_A$* phase for 'm' = 7. These results conclude that the length of the

(-CH_2-)$_m$ flexible chain influences the polymorphism of the smectic phases, and the vitrification and crystallization processes.

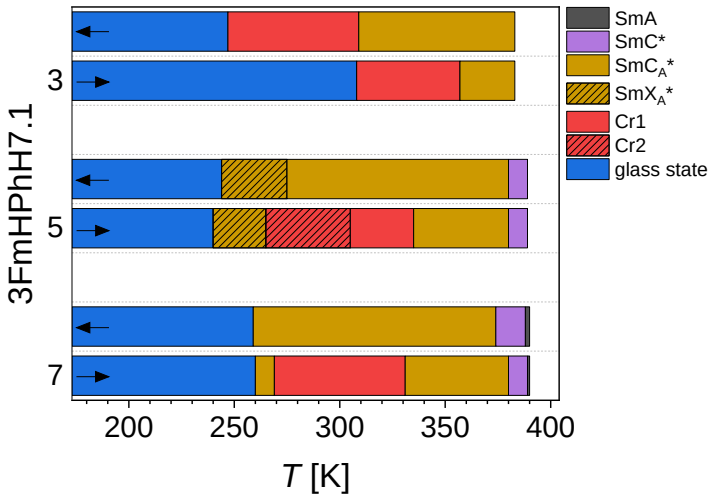

Figure 11. Phase transitions of the 3FmHPhH7.1 compounds during fast cooling and heating. The transition temperatures of 3F3HPhH7.1 are taken from Ref. [66], of 3F5HPhH7.1 from Refs. [70,71] and of 3F7HPhH7.1 from Refs. [15,67,69,72].

The parameters of both cold- and melt crystallization as well as of glass transition for all 3FmHPhH7.1 isomers, are presented in Tab. 2. The cold crystallization under non-isothermal conditions is analysed based on DSC (Eq. 5) results using the Ozawa model (Eq. 6). This process depends mainly on the thermodynamic factor and occurs with the one-dimensional crystal growth according to POM observations (n_O = 0.6-1.1) for the 3F3HPhH7.1 compound [66]. For the 3F5HPhH7.1 and 3F7HPhH7.1 samples, the non-isothermal cold crystallization is a complex phenomenon controlled mainly by diffusion for slow heating and thermodynamic factor for fast heating. The dimensionalities of the obtained crystals Cr1 and Cr2 for 3F5HPhH7.1 are different depending on the applied heating rate of the sample (n_O = 0.7-4.0) [71], while for 3F7HPhH7.1 there is three-dimensional growth of the crystal Cr1 according to POM observations (n_O = 2.5-3.0) [15]. The activation energies of non-isothermal cold crystallization for 'm' = 3 determined based on the Kissinger (Eq. 7) and Augis-Bennett (Eq. 8) formulas are 256 kJ mol^{-1} and 247 kJ mol^{-1}, respectively [66]. For 'm' = 5, two different linear dependences for slow and fast heating confirm two mechanisms of cold crystallization with E_A = 146-158 kJ mol^{-1} for slow heating and over 60 kJ mol^{-1} for fast heating [71]. Similarly, for 'm' = 7, the activation energy is higher for slow heating (E_A = 130 kJ mol^{-1}) than for fast heating (E_A = 50 kJ mol^{-1}) [15]. The kinetics of isothermal

cold crystallization is described for 3F5HPhH7.1 based on DSC (Eq. 9) and BDS (Eq. 10) results, and for 3F7HPhH7.1 also on FTIR (Eq. 11) results, using the Avrami model (Eq. 12). The thermal history of the sample has an impact on the nature of this process for 3F5HPhH7.1 [71]. Interestingly, the two-step crystallization under isothermal conditions occurs according to the measurements performed during fast heating with the rates of 2-5 K min^{-1} (Fig. 12a) and depends mainly on a diffusion rate. The mechanism of the first step corresponds to three-dimensional crystal growth (n_A = 3.3-4.0) with the activation energy of 135 kJ mol^{-1}, while for the second step the growth of the crystal phase is two-dimensional (n_A = 2.2-2.8) and E_A = 146 kJ mol^{-1}. The slower heating of the 'm' = 5 sample indicates a change in the nature of this phenomenon from the two-step to one-step process, occurring with the two-dimensional growth of crystallites (n_A = 2.2). For 3F7HPhH7.1 [69], the isothermal cold crystallization in a one-route process occurs with three-dimensional growth of nuclei according to POM observations (n_A = 2.8-3.1) and depends primarily on a diffusion rate with the activation energy of 133 kJ mol^{-1}.

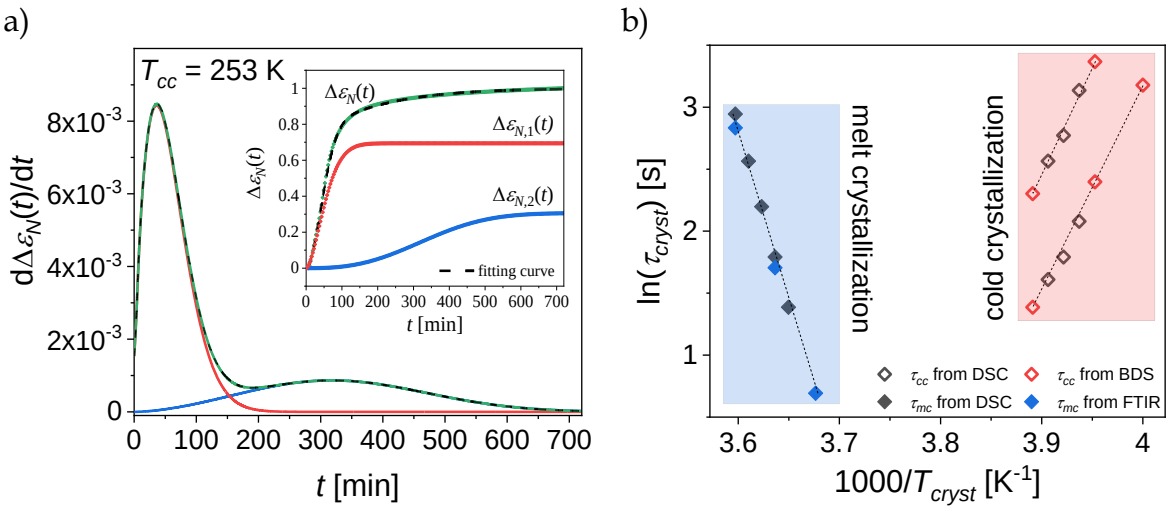

Figure 12. The BDS spectra measured upon isothermal cold crystallization [71] (a) and activation plots for both routes of isothermal cold (empty symbols) and melt (solid symbols) crystallization [71] (b) of 3F5HPhH7.1. Reproduced from Ref. [71] with permission from the Royal Society of Chemistry.

We also analyse the correlation between the crystallization rate and molecular mobility by comparing the characteristic crystallization time τ and the α-relaxation time τ_α (Fig. 13), according to Eq. 4. For both compounds with 'm' = 5 and 7, the coupling coefficient is below 0.5, meaning a mainly diffusion-controlled cold crystallization, which is analysed using the Avrami model. The melt crystallization

under isothermal conditions is also described using the Avrami model (Eq. 12), based on DSC and FTIR results for 3F5HPhH7.1 as well as DSC and POM results for 3F7HPhH7.1. This is a thermodynamic-controlled process with three-dimensional crystal growth for both 'm' = 5 (n_A = 3.5-4.2) [71] and 'm' = 7 (n_A = 3.2-3.5, E_A = 51 kJ mol^{-1}) [67] compounds. The nature of changes in the crystallization times (τ_{cryst}) vs the crystallization temperatures (T_{cryst}) of 3F5HPhH7.1 proves that the isothermal cold crystallization is driven by diffusion, while the melt crystallization is controlled by thermodynamic factor (Fig. 12b). The dependences plotted based on DSC, BDS and FTIR measurements coincide for each other.

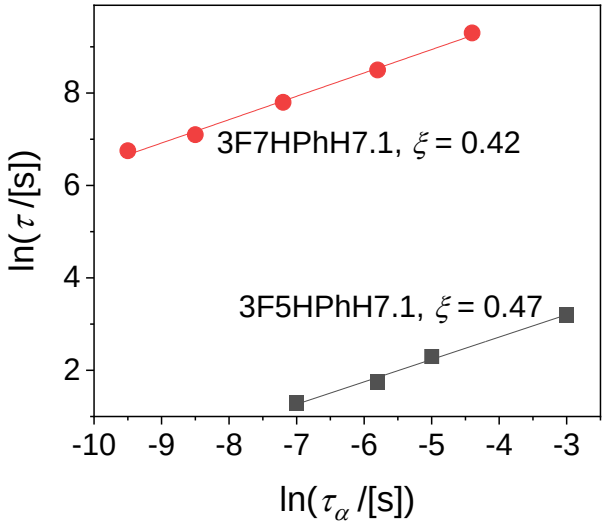

Figure 13. Coupling between the crystallization time and the α-relaxation time of the 3FmHPhH7.1 compounds. The data results of 3F5HPhH7.1 are taken from Ref. [71], of 3F7HPhH7.1 from Ref. [69].

The 'm' = 3 compound vitrifies from the CONDIS crystal phase, while for longer homologues the glass transition is observed from the SmX_A^* phase for 'm' = 5 and from the SmC_A^* phase for 'm' = 7. The dielectric spectra are obtained for the 'm' = 5 and 7 samples upon heating after fast cooling. The α-process, typical for materials undergoing vitrification, occurs for both compounds and it is described by the HN model (Eq. 1). The values of T_g deduced by fitting the VFT temperature relationship to the α-relaxation times of (Eq. 2) are equal to T_g = 242 K for 3F5HPhH7.1 [71] and $T_{g,1}$ = 259 K and $T_{g,2}$ = 239 K for 3F7HPhH7.1 [69]. The values of the m_f parameter, calculated according to Eq. 3, are similar for both homologues and equal to m_f = 146 for 'm' = 5 and $m_{f,1}$ = 150 and $m_{f,2}$ = 136 for 'm' = 7, indicating that both compounds are fragile glass-forming systems. Considering the value of T_g = 247 K for 'm' = 3

determined from DSC results and the second glass transition for 'm' = 7 we assume that T_g decreases as the oligomethylene spacer length increases, similarly as for polymers [73]. This behaviour proves a connection between the glass transition and the intramolecular chain motions.

Table 2. Parameters of cold- and melt crystallization as well as glass transition of the 3FmHPhH7.1 compounds. The data results of 3F3HPhH7.1 are taken from Ref. [66], of 3F5HPhH7.1 from Ref. [71] and of 3F7HPhH7.1 from Refs. [15,67,69].

3FmHPhH7.1	'm' = 3	'm' = 5	'm' = 7
Non-isothermal cc	n_O = 0.6-1.1 E_A = 247-265 kJ mol^{-1} mechanism: thermodynamic	n_O = 0.7-4.0 E_A = 60-158 kJ mol^{-1} mechanism: diffusion (slow heating), thermodynamic (fast heating)	n_O = 2.5-3.0 E_A = 50-130 kJ mol^{-1} mechanism: diffusion (slow heating), thermodynamic (fast heating)
Isothermal cc		n_A = 2.2-4.0 (fast heating) n_A = 2.2 (slow heating) E_A = 135-146 kJ mol^{-1} mechanism: diffusion	n_A = 2.8-3.1 E_A = 133 kJ mol^{-1} mechanism: diffusion
Isothermal mc		n_A = 3.5-4.2 mechanism: thermodynamic	n_A = 3.2-3.5 E_A = 51 kJ mol^{-1} mechanism: thermodynamic
Glass transition	from Cr1 T_g = 247 K	from SmX_A* T_g = 242 K m_f = 146	from SmC_A* $T_{g,1}$ = 259 K $m_{f,1}$ = 150 $T_{g,2}$ = 239 K $m_{f,2}$ = 136

4. Influence of the rigid core structure ('X_1' and 'X_2' parameters)

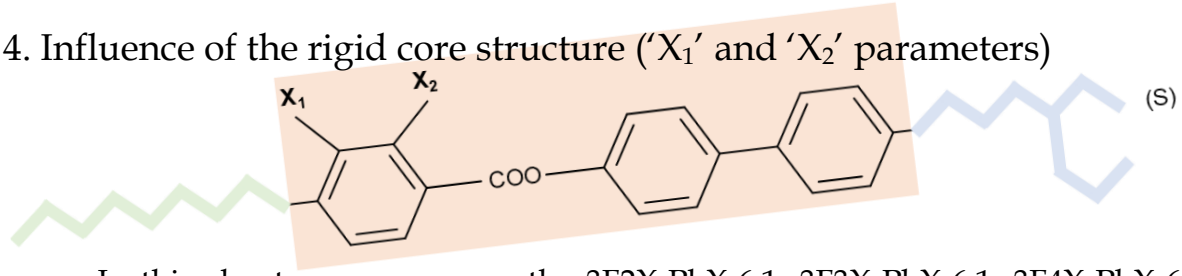

In this chapter, we compare the 3F2X_1Ph$X_2$6.1, 3F3X_1Ph$X_2$6.1, 3F4X_1Ph$X_2$6.1, 3F5X_1Ph$X_2$6.1, 3F6X_1Ph$X_2$6.1 and 3F7X_1Ph$X_2$6.1 compounds, which differ in the fluorosubstitution of the phenyl ring in the rigid core ('X_1' = H, F, 'X_2' = H, F). Their phase behaviour, depending on the heating/cooling rates, is described in Chapter 3.1. The summary of the phase situations for cooling/heating is shown in Fig. 14a (for 3F2X_1Ph$X_2$6.1), Fig. 14b (for 3F3X_1Ph$X_2$6.1), Fig. 14c (for 3F4X_1Ph$X_2$6.1), Fig. 14d (for 3F5X_1Ph$X_2$6.1), Fig. 14e (for 3F6X_1Ph$X_2$6.1) and Fig. 14f (for 3F7X_1Ph$X_2$6.1), taking into account various combination of H and F substituents. The exact values of the phase transition temperatures are given in Tab 5. For all series, the change of the phase transition temperatures is visible, when the phenyl ring is substituted with one or two fluorine atoms, e.g. for all 'm' values, the 3FmHPhF6.1 series has lower transition temperatures than 3FmHPhH6.1. The impact of the rigid core structure -X_1PhX_2- ('X_1' = H, F, 'X_2' = H, F) on the vitrification, is observed for longer homologues with 'm' = 5-7.

In all compounds, the SmC_A* phase appears. The SmA phase is observed for homologues with 'm' ≥ 4, and the SmC for those with 'm' = 2, 4-7. The crystal phase polymorphism has been detected for all compounds except 3F7FPhH6.1. The vitrification has been found in homologues with 'm' = 5, 7 and also in 3F6HPhF6.1. The transition to the hexatic SmX_A* phase is observed for MHPOBC [74] and some MHPOBC-based compounds with a partially fluorinated terminal chain, namely for 1F7 [75,76], 3F6Bi [13], 4H6 [77], 3F4HPhH6.1 [48], 3F5HPhH6.1 [49], 3F7HPhH6.1 [51] and 3F5HPhH7.1 [70]. Most of these compounds (except 1F7) are not fluorosubstituted in the rigid core. There is an assumption that fluorination of the phenyl ring prevents the formation of the hexatic smectic phase.

Compounds of the 3FmX_1Ph$X_2$6.1 series ('m' = 2, 3) exhibit an identical phase sequence, regardless of the type of fluorosubstitution of the phenyl ring. Compounds with 'm' = 2 form the SmC*, SmC_A* and crystal phases (especially 3F2HPhF6.1 forms two crystal phases), while compounds with 'm' = 3 exhibit the Cr and SmC_A* phases.

The results obtained for 3F4HPhH6.1 and 3F4FPhF6.1 show that the double fluorosubstitution facilitates crystallization. The Iso – SmC* and SmC* - SmC_A* transition temperatures of 3F4FPhF6.1 are lower than in 3F4HPhH6.1. On the contrary, the fluorosubstitution in the rigid core increases the crystallization and melting temperatures.

For 3F5HPhF6.1 and 3F5FPhF6.1, fluorosubstituted at the X_2 position, the glass transition of the SmC_A* phase during cooling followed by cold crystallization during heating is reported. For 3F5HPhH6.1, the vitrification from the more ordered SmX_A* phase is visible. The 3F5FPhH6.1 crystallizes even upon fast cooling, unlike the remaining compounds of the $3F5X_1PhX_2$6.1 series. These results show that fluorosubstitution of the phenyl ring significantly influences the glass forming properties of the $3F5X_1PhX_2$6.1 compounds. The fluorosubstitution at the X_1 position leads to easier crystallization, while fluorosubstitution at the X_2 position increases the tendency to the formation of the smectic glass upon cooling.

Among compounds of the $3F6X_1PhX_2$6.1 series, only 3F6HPhF6.1 is a glass former. Compounds with the H atom at the X_2 position exhibit on heating the same sequence of the smectic phases: SmC_A* - SmC* - SmA*, but the phase transition temperatures of 3F6FPhH6.1 are shifted towards lower temperatures in respect to 3F6HPhH6.1. The fluorosubstituted compound starts crystallizing at smaller undercooling for a low cooling rate (2 K min^{-1}), while for fast cooling (5-20 K min^{-1}) the crystallization of the non-fluorosubstituted compound occurs faster.

The rigid core structure affects the phase behaviour of the $3F7X_1PhX_2$6.1 compounds. Two homologues with a single F atom in the phenyl ring, 3F7HPhF6.1 and 3F7FPhH6.1, vitrify upon cooling and form the glass of the SmC_A* phase. For these compounds, crystallization is never observed upon cooling. The double-fluorinated 3F7FPhF6.1 forms a crystal phase upon cooling even for rates up to 20 K min^{-1}. The 3F7HPhF6.1 compound undergoes cold crystallization, dependent significantly on the diffusion rate, while 3F7FPhF6.1 undergoes melt crystallization, controlled by the thermodynamic driving force. The lack of melt crystallization of 3F7HPhF6.1, even upon slow cooling, may arise, e.g. from the lower melting temperature of the crystal phase, which results in the lower thermodynamic driving force of crystallization compared to 3F7FPhF6.1.

The tendency to create the glass of the smectic phase (SmX_A* or SmC_A*) is observed for various types of fluorosubstitution. However, the F atom at the X_2 position facilitates the most vitrification, e.g. decreases the glass transition temperature and increases the cold crystallization rate.

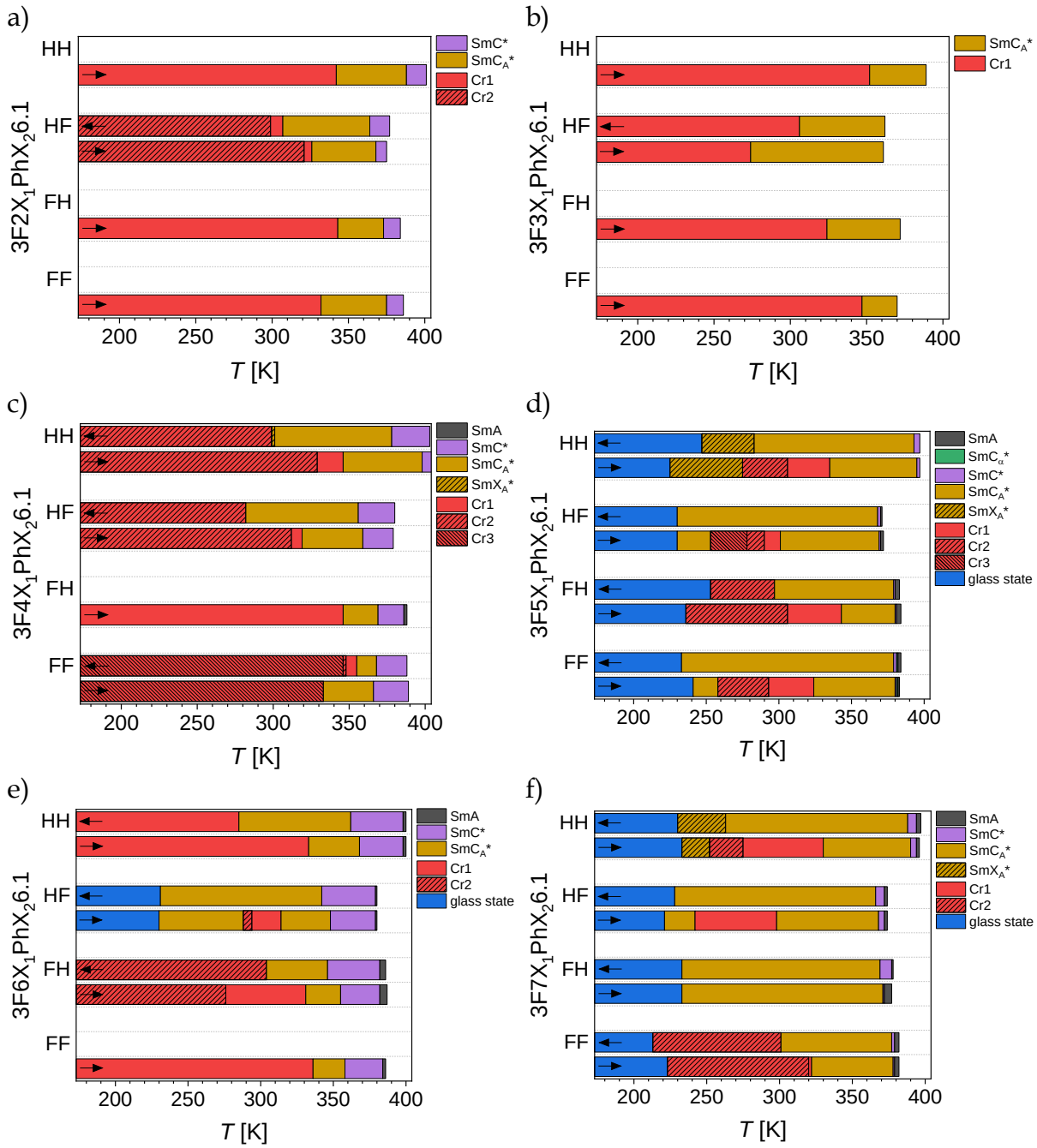

Figure 14. Phase transitions of the $3F2X_1PhX_26.1$ (a), $3F3X_1PhX_26.1$ (b), $3F4X_1PhX_26.1$ (c), $3F5X_1PhX_26.1$ (d), $3F6X_1PhX_26.1$ (e) and $3F7X_1PhX_26.1$ (f) compounds during fast cooling and heating.

5. Influence of the chiral alkyl chain length ('r' parameter)

In this chapter, we compare the 3F3HPhHr.1, 3F5HPhHr.1, 3F7HPhHr.1 and 3F5HPhFr.1 compounds, which differ in the length of the chiral chain ('r' = 4, 6, 7). The phase behaviour of 3FmHPhHr.1 ('m' = 3, 5, 7; 'r' = 6, 7), and 3F5HPhF6.1, depending on the heating/cooling rates, is described in Chapter 3. The summary of the phase situations for cooling/heating is shown in Fig. 15a (for 3F3HPhHr.1), Fig. 15b (for 3F5HPhHr.1) and Fig. 15c (for 3F7HPhHr.1) for 'r' = 6 and 7, and Fig. 15d (for 3F5HPhFr.1) for 'r' = 4 and 6. The exact values of the phase transition temperatures are given in Tab 5. According to DSC results, 3F5HPhF4.1 vitrifies from the SmC_A^* phase even upon slow cooling: Iso (388 K) SmA* (385 K) SmC* (374 K) SmC_A^* (T_g = 232 K) $gSmC_A^*$. Upon subsequent heating, the phase sequence is like during cooling if heating rates are higher than 1.5 K min^{-1}. However, during slow heating with the rates of ≤ 1.5 K min^{-1}, the cold crystallization occurs: $gSmC_A^*$ (~235 K) SmC_A^* (T_{cc} = 266 K) Cr (286 K) SmC_A^*, which is not presented in Fig. 15d.

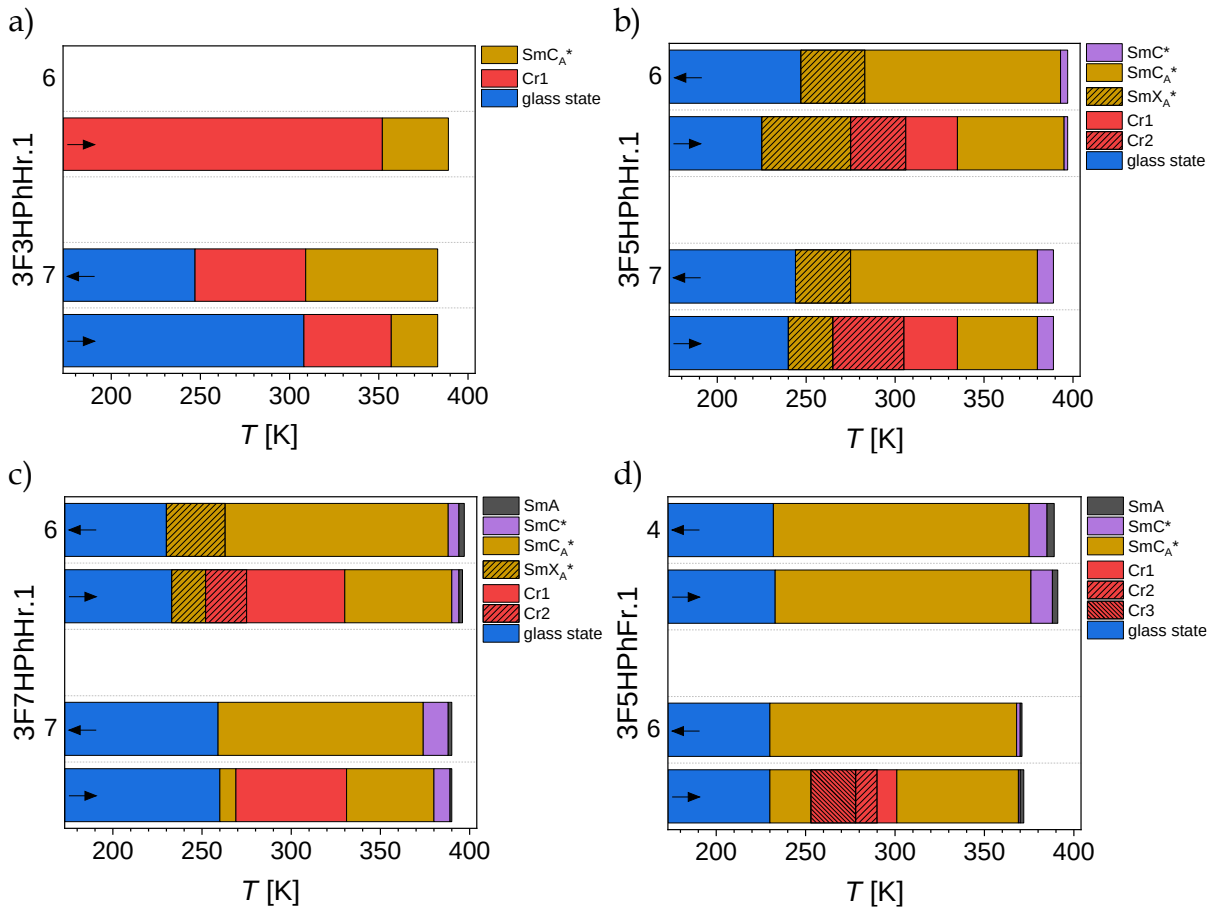

Figure 15. Phase transitions of the 3F3HPhHr.1 (a), 3F5HPhHr.1 (b), 3F7HPhHr.1 (c) and 3F5HPhFr.1 (d) compounds during fast cooling and heating.
The transition temperatures of 3F5HPhF4.1 are taken from Refs. [12,78,79].

In each group of compounds, the transition temperature to the isotropic phase is higher for the compound with a shorter chiral chain. Additionally, with an increase of the 'r' parameter, the temperature range of the SmC_A^* phase occurrence decreases. Both compounds of the 3F3HPhHr.1 ('r' = 6, 7) series have a similar phase sequence (Cr – SmC_A^*). A compound with 'r' = 7 undergoes glass transition from the CONDIS crystal phase upon cooling. A compound with 'r' = 6 only crystallizes, however measurements are performed only upon slow cooling of this sample to 273 K. Homologues of the 3F5HPhHr.1 ('r' = 6, 7) series also have an identical phase behaviour both upon cooling (SmC* - SmC_A^* - SmX_A^* - $gSmX_A^*$) and heating ($gSmX_A^*$ - SmX_A^* - Cr2 – Cr1 – SmC_A^* - SmC*) of the samples. Among these compounds, with an increase of the 'r' parameter, the temperature range of the SmC* phase occurrence increases, and the values of T_g and T_{cc} decrease. Significant differences in the phase behaviour are evident for compounds of the 3F7HPhHr.1 ('r' = 6, 7) series. A compound with 'r' = 7 has a broader SmC* phase occurrence temperature range and higher T_g and T_{cc} temperatures than its shorter homologue. On the other hand, a compound with 'r' = 6 exhibits a richer polymorphism of crystal phases and vitrifies from the SmX_A^* phase, unlike a compound with 'r' = 7, which undergoes vitrification from the SmC_A^* phase. For compounds of the 3F5HPhFr.1 ('r' = 4, 6) series, a reduction in the temperature range of the SmC* phase occurrence is observed, and up to three crystal phases appear upon heating of a compound with 'r' = 6 compared to its shorter homologue with 'r' = 4.

The comparison of the glass transition as well as the cold- and melt crystallization for the 3F5HPhFr.1 ('r' = 4, 6) compounds is shown in Tab. 3. The kinetics of both phenomena for 3FmHPhHr.1 ('m' = 3, 5, 7; 'r' = 6, 7), and also for 3F5HPhF6.1 is discussed in details in Chapter 3. The non-isothermal cold crystallization of 3F5HPhF4.1 is described based on DSC and BDS measurements. According to the Ozawa model (Eq. 6), the cold crystallization under non-isothermal conditions is driven by two different mechanisms, i.e. thermodynamic factor with a large dispersion of crystal growth dimensionality (n_O = 0.2-2.4) for slow heating rates, and kinetic factor with varying characteristic of crystal growth (n_O = 3.0-4.9) for fast heating rates [12]. According to the Kissinger (Eq. 7) and Augis-Bennett (Eq. 8)

models, the activation energy of this process is E_A = 51 kJ mol^{-1}, which is smaller than found for non-isothermal cold crystallization from the nematic phase [16], higher than in case of the crystallization from the SmC$_A$* phase for a similar compound [55], and comparable with the value found for that process from the chiral nematic phase [80]. The kinetics of the isothermal cold crystallization of 3F5HPhF4.1 is defined based on DSC, POM and BDS measurements, according to the Avrami formula (Eq. 12). There are two different crystallization mechanisms: kinetic below 257 K with E_A = 70-100 kJ mol^{-1} and thermodynamic above 257 K with E_A = 50-69 kJ mol^{-1}, both occurring with two-dimensional plate growth according to POM observations with a constant nucleation rate (n_A = 2.1-2.4) [79] and with the coupling coefficient of ξ = 0.50 (Fig. 16), calculated according to Eq. 4. On the other hand, the isothermal cold crystallization of 3F5HPhF6.1 [53], having longer alkyl chain than 3F5HPhF4.1, occurs with one-dimensional growth of needle-like crystallites seen by optical observations (n_A = 1.2) and E_A = 48 kJ mol^{-1} as well as ξ = 0.26. The activation energy and the coupling coefficient are smaller for a compound with 'r' = 6 than for a compound with 'r' = 4, indicating that the nucleation rate influences the crystallization kinetics more for longer homologue. However, the diffusion rate still has a more prominent role.

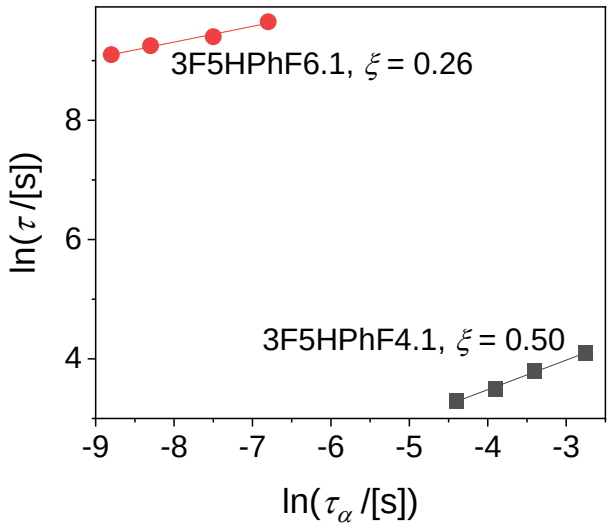

Figure 16. Coupling between the crystallization time and the α-relaxation time of the 3F5HPhFr.1 compounds. The data results of 3F5HPhF4.1 are taken from Ref. [79], of 3F5HPhF6.1 from Ref. [53].

Both 3F5HPhFr.1 compounds vitrify from the SmC$_A$* phase. Fitting of the VFT formula (Eq. 2) to the relaxation time of the α-process gives almost identical values of T_g and m_f for both homologues: T_g = 232-234 K and m_f = 116-148 for 3F5HPhF4.1, and

T_g = 230 K and m_f = 107 for 3F5HPhF6.1. Both compounds are fragile glass formers, but the fragility index is smaller for a compound with 'r' = 6 than for a compound with 'r' = 4, which implies that 3F5HPhF6.1 should crystallize easier. The opposite situation is observed for the 3F5HPhHr.1 and 3F7HPhHr.1 series, at which the fragility index is higher for longer homologues with 'r' = 7 than for compounds with 'r' = 6 (Tabs. 1,2). It means that one should consider not only the chiral chain length but also the fluorosubstitution of the phenyl ring, which affects the behaviour of the $3FmX_1PhX_2r.1$ compounds.

Table 3. Parameters of cold- and melt crystallization as well as glass transition of the 3F5HPhFr.1 compounds ('r' = 4, 6). The data results of 3F5HPhF4.1 are taken from Refs. [12,78,79], of 3F5HPhF6.1 from Ref. [53].

3F5HPhFr.1	'r' = 4	'r' = 6
Non-isothermal cc	n_O = 0.2-2.4 (slow heating) n_O = 3.0-4.9 (fast heating) E_A = 51 kJ mol^{-1} mechanism: thermodynamic (slow heating), kinetic (fast heating)	
Isothermal cc	n_A = 2.1-2.4 E_A = 50-100 kJ mol^{-1} mechanism: kinetic (low T), thermodynamic (high T)	n_A = 1.2 E_A = 48 kJ mol^{-1} mechanism: diffusion
Glass transition	from SmC_A* $T_{g,1}$ = 234 K $m_{f,1}$ = 116 $T_{g,2}$ = 232 K $m_{f,2}$ = 148	from SmC_A* T_g = 230 K m_f = 107

6. Influence of the type of the chiral centre ('r' and 's' parameters)

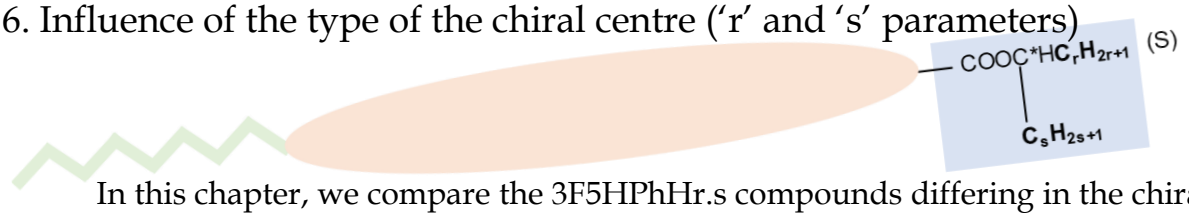

In this chapter, we compare the 3F5HPhHr.s compounds differing in the chiral centre, based on (*S*)-(+)-2-octanol ('r.s' = 6.1) and (*S*)-(+)-3-octanol ('r.s' = 5.2). According to DSC results, 3F5HPhH5.2 exhibits the same phase situation for both slow and fast heating/cooling rates, constantly undergoing vitrification from the SmC_A^* phase without crystallization, even during slow cooling. The phase behaviour upon cooling with the rate of 2 K min^{-1} is: Iso (363 K) SmA* (363 K) SmC_A^* (T_g = 236 K) $gSmC_A^*$, while upon heating with the same rate is: $gSmC_A^*$ (~238 K) SmC_A^* (T_{cc} = 272 K) Cr (334 K) SmC_A^* (364 K) Iso. The phase behaviour of 3F5HPhH6.1 depends on the heating/cooling rates, which is described in Chapter 3.1. The comparison of the phase situations for fast cooling/heating rates of both 3F5HPhHr.s compounds is shown in Fig. 17. The exact values of the phase transition temperatures are given in Tab 5. The 'r.s' = 6.1 isomer exhibits the SmC* phase instead of SmA* and it also forms the glass of the more ordered, hexatic SmX_A^* phase. The 'r.s' = 5.2 compound has a high tendency to vitrification because the $gSmC_A^*$ state is obtained even with slow cooling with the rate of 2 K min^{-1}. In comparison, the 'r.s' = 6.1 compound crystallizes during cooling at this rate and to obtain the $gSmX_A^*$ state, cooling with the rate of ≥ 5 K min^{-1} is necessary. The different lengths of the aliphatic chains attached to the chiral carbon atom may lead to distinct distributions of the most energetically favourable molecular conformations of both homologues ('r.s' = 5.2 and 6.1) as the temperature changes. As a result, this variation in conformational distribution may influence the observed phase behaviour.

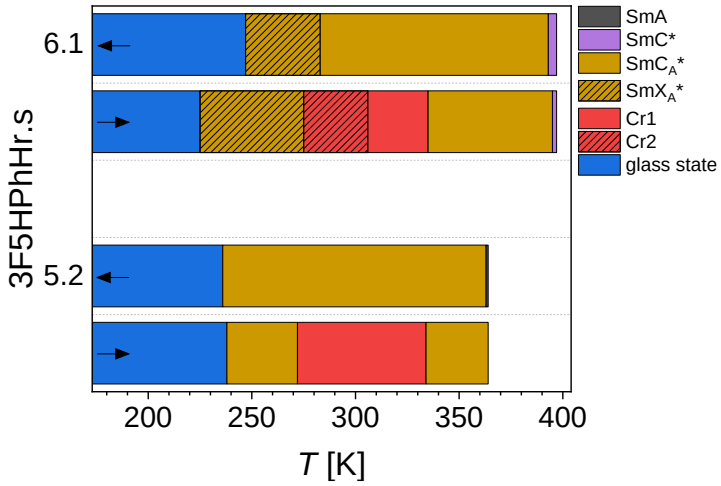

Figure 17. Phase transitions of the 3F5HPhHr.s compounds during fast cooling and heating. The transition temperatures of 3F5HPhH5.2 are taken from Ref. [20].

In Tab. 4, data concerning vitrification and cold- and melt crystallization for the 3F5HPhHr.s compounds have been compiled. The kinetics of both phenomena for 3F5HPhH6.1 is discussed in details in Chapter 3.1. The kinetics of the cold crystallization of 3F5HPhH5.2 under non-isothermal conditions is described based on DSC measurements. According to the Ozawa model (Eq. 6), this process depends mostly on the diffusion rates and occurs with crystals' spherulitic/sheaf growth according to POM observations (n_O = 6.3) [20]. By comparing the characteristic crystallization time τ and the α-relaxation time τ_α (Fig. 18), we can determine to what extent the crystallization kinetics is controlled by diffusion, according to Eq. 4. For both compounds, the coupling coefficient is close to 1, meaning a mainly diffusion-controlled cold crystallization, which is confirmed by analysis using the Ozawa model. According to the Kissinger (Eq. 7) and Augis-Bennett (Eq. 8) models, for 3F5HPhH5.2 there are three regimes of cold crystallization, with the activation energy decreasing with increasing heating rates: E_A = 113 kJ mol^{-1} for 2-5 K min^{-1} heating rates, E_A = 68 kJ mol^{-1} for 5-15 K min^{-1} heating rates and E_A = 37 kJ mol^{-1} for 15-30 K min^{-1} heating rates. The kinetics of isothermal cold crystallization for 3F5HPhH5.2 is presented based on DSC and BDS results. According to the Avrami model (Eq. 12), cold crystallization is a diffusion-controlled process with two-dimensional crystal growth (n_A = 2.0-2.8) and the activation energy value equals 108 kJ mol^{-1} based on DSC results, as well as depends mostly on diffusion with three-dimensional crystal growth (n_A = 2.6-3.0) and the activation energy value equals to 172 kJ mol^{-1} based on BDS results [20]. The melt crystallization of 3F5HPhH5.2 under isothermal conditions is

discussed based on DSC and POM results using the Avrami model (Eq. 12). The thermodynamic driving force mainly influences the kinetics of this process at larger undercooling. In comparison, at smaller undercooling, it is equally affected by the rate of the diffusion and the formation of new nuclei. The growth of crystallites is two-dimensional for smaller undercooling (n_A = 2.6-2.7), and it decreases at lower temperatures (n_A = 1.7-2.0) [20]. The activation energy is 537 kJ mol^{-1}. Such a high energy barrier for crystallization corresponds to easier vitrification of the smectic phase than the crystal phase.

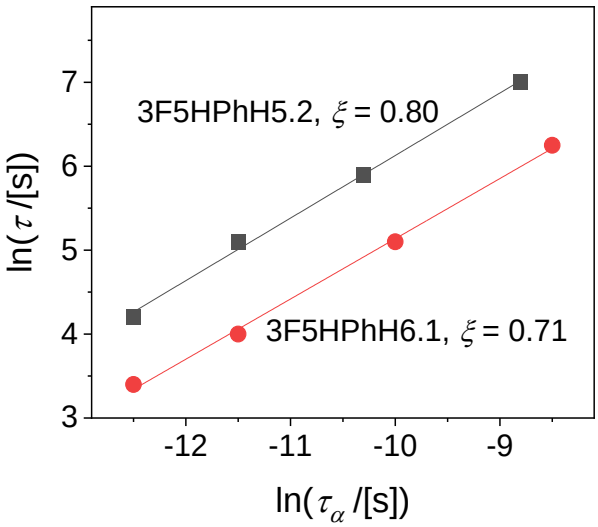

Figure 18. Coupling between the crystallization time and the α-relaxation time of the 3F5HPhHr.s compounds. The data results of 3F5HPhH6.1 are taken from Ref. [49], of 3F5HPhH5.2 from Ref. [20].

The 'r.s' = 5.2 isomer vitrifies from the SmC_A^* phase upon slow and fast cooling, while for the 'r.s' = 6.1 sample the glass transition is observed from the SmX_A^* phase only upon fast cooling. The α-process occurs at glass forming phases of both compounds in BDS spectra recorded upon heating after fast cooling and it is described by the HN model (Eq. 1). The T_g values determined by fitting the VFT formula to the α-relaxation times (Eq. 2) are almost identical for both isomers, T_g = 238 K for 3F5HPhH5.2 and 237 K for 3F5HPhH6.1. The m_f parameter, according to Eq. 3, is equal to 139 for 3F5HPhH5.2 (making this compound a very fragile glass former) and 89 for 3F5HPhH6.1 (therefore, this compound has an average fragility). Compounds with a higher fragility index tend to undergo crystallization more readily [81], however in our case, 3F5HPhH5.2 demonstrates an interesting exception. Despite having a higher

fragility index, it exhibits a superior ability to form a glass, making it more resistant to crystallization.

Table 4. Parameters of cold- and melt crystallization as well as glass transition of the 3F5HPhHr.s compounds. The data results of 3F5HPhH6.1 are taken from Ref. [49], of 3F5HPhH5.2 from Ref. [20].

3F5HPhHr.s	'r.s' = 5.2	'r.s' = 6.1
Non-isothermal cc	n_O = 6.3 E_A = 37-113 kJ mol^{-1} mechanism: diffusion	n_O = 3.1 E_A = 73-141 kJ mol^{-1} mechanism: diffusion (low T), diffusion + thermodynamic (high T)
Isothermal cc	n_A = 2.0-3.0 E_A = 108-172 kJ mol^{-1} mechanism: diffusion	
Isothermal mc	n_A = 1.7-2.7 E_A = 537 kJ mol^{-1} mechanism: thermodynamic (larger undercooling), diffusion and thermodynamic (smaller undercooling)	n_A = 2.7-2.9 mechanism: thermodynamic
Glass transition	from SmC_A* T_g = 238 K m_f = 139	from SmX_A* T_g = 237 K m_f = 89

Table 5. Temperatures of phase transitions of the 3FmX$_1$PhX$_2$r.s compounds upon slow heating (1st line), slow cooling (2nd line), fast heating (3rd line) and fast cooling (4th line).

Compound	glass	*T* [K]	Cr3	*T* [K]	Cr2	*T* [K]	Cr1	*T* [K]	SmX$_A$*	*T* [K]	SmC$_A$*	*T* [K]	SmC*	*T* [K]	SmC$_\alpha$*	*T* [K]	SmA*	*T* [K]	Iso
3F2HPhH6.1	-		-		-		*	342	-		*	388	*	401	-		-		*
3F3HPhH6.1	-		-		-		*	352	-		*	389	-		-		-		*
3F4HPhH6.1	-		-		*	329	*	346	-		*	381	*	403	-		-		*
	-		-		*	299	-		*	301	*	378	*	403	-		-		*
3F5HPhH6.1	-		-		*	293	*	335	-		*	395	*	397	-		-		*
	-		-		*	276	-		*	283	*	393	*	397	-		-		*
	*	(softening at ~225) 275	-		*	306	*	335	-		*	395	*	397	-		-		*
	*	247	-		-		-		*	283	*	393	*	397	-		-		*
3F6HPhH6.1	-		-		-		*	333	-		*	368	*	398	-		*	400	*
	-		-		-		*	285	-		*	362	*	398	-		*	400	*
3F7HPhH6.1	*	(softening at ~233) 252	-		*	275	*	330	-		*	390	*	394	-		*	396	*
	*	230	-		-		-		*	263	*	388	*	394	-		*	397	*
3F2HPhF6.1	-		-		-		*	326	-		*	368	*	375	-		-		*
	-		-		*	321	*	326	-		*	368	*	375	-		-		*
	-		-		*	299	*	307	-		*	364	*	377	-		-		*
3F3HPhF6.1	-		-		-		*	306	-		*	362	-		-		-		*
3F4HPhF6.1	-		-		*	312	*	319	-		*	359	*	379	-		-		*
	-		-		*	282	-		-		*	356	*	380	-		-		*
3F5HPhF6.1	*	(softening at ~230) 253	*	278	*	290	*	301	-		*	369	*	370	-		*	372	*
	*	230	-		-		-		-		*	368	*	370	-		*	371	*
3F6HPhF6.1	*	(softening at ~230) 288	-		*	294	*	314	-		*	348	*	379	-		*	380	*
	*	231	-		-		-		-		*	342	*	379	-		*	380	*
3F7HPhF6.1	*	(softening at ~221) 242	-		-		*	298	-		*	368	*	372	-		*	374	*
	*	221	-		-		-		-		*	366	*	372	-		*	374	*
3F2FPhH6.1	-		-		-		*	343	-		*	373	*	384	-		-		*
3F3FPhH6.1	-		-		-		*	324	-		*	372	-		-		-		*
3F4FPhH6.1	-		-		-		*	346	-		*	369	*	386	-		*	388	*
3F5FPhH6.1	*	(softening at ~236) 326	-		-		*	343	-		*	380	*	380	-		*	383	*
	*	253	-		*	297	-		-		*	379	*	380	-		*	383	*
3F6FPhH6.1	-		-		*	276	*	331	-		*	355	*	382	-		*	387	*
	-		-		*	304	-		-		*	346	*	382	-		*	386	*

3F7FPhH6.1	*	(softening at ~233) 280	-		*	292	*	304	-		*	371	*	372	*	372	*	377	*
	*	233	-		-		-		-		*	369	*	371	*	376	*	377	*
	*	softening at ~233	-		-		-		-		*	371	*	372	-		*	377	*
	*	233	-		-		-		-		*	369	*	376	-		*	377	*
3F2FPhF6.1	-		-		-		*	332	-		*	375	*	386	-		-		*
3F3FPhF6.1	-		-		-		*	347	-		*	370	-		-		-		*
3F4FPhF6.1	-		*	346	*	348	*	355	-		*	368	*	388	-		-		*
	-		*	333	-		-		-		*	366	*	389	-		-		*
3F5FPhF6.1	-		-		-		*	327	-		*	380	*	381	*	381	*	382	*
	-		-		-		*	296	-		*	379	*	381	*	381	*	383	*
	*	(softening at ~241) 258	-		*	293	*	324	-		*	380	*	381	*	381	*	382	*
	*	233-238	-		-		-		-		*	379	*	381	*	381	*	383	*
3F6FPhF6.1	-		-		-		*	336	-		*	358	*	384	-		*	386	*
3F7FPhF6.1	*	softening at ~223	-		*	320	*	322	-		*	378	*	379	-		*	382	*
	*	213	-		*	301	-		-		*	377	*	379	-		*	382	*
3F3HPhH7.1																			
	-		-		-		*	320	-		*	383	-		-		-		*
	*	softening at ~308	-		-		*	357	-		*	383	-		-		-		*
	*	247	-		-		*	309	-		*	383	-		-		-		*
3F5HPhH7.1	-		-		*	300	*	335	-		*	380	*	389	-		-		*
	-		-		*	270	-		*	279	*	380	*	389	-		-		*
	*	(softening at ~240) 265	-		*	305	*	335	-		*	380	*	389	-		-		*
	*	244	-		-		-		*	275	*	380	*	389	-		-		*
3F7HPhH7.1	-		-		-		*	331	-		*	380	*	389	-		*	390	*
	-		-		-		*	286	-		*	374	*	388	-		*	390	*
	*	(softening at ~260) 269	-		-		*	331	-		*	380	*	389	-		*	390	*
	*	239, 259	-		-		-		-		*	374	*	388	-		*	390	*
3F5HPhF4.1	*	(softening at ~235) 266	-		-		*	286	-		*	377	*	386	-		*	388	*
	*	232	-		-		-		-		*	374	*	385	-		*	388	*
	*	softening at ~233	-		-		-		-		*	376	*	388	-		*	391	*
	*	232	-		-		-		-		*	375	*	385	-		*	389	*
3F5HPhH5.2	*	(softening at ~238) 272	-		-		*	334	-		*	364	-		-		-		*
	*	236	-		-		-		-		*	363	-		-		*	363	*

7. Conclusions

Investigations of the compounds from the 3FmX_1PhX_2r.s family (where 'm' = 2-7, 'X_1', 'X_2' = H, F, 'r' = 4-7, 's' = 1, 2) prove that the molecular structure, e.g. the oligomethylene chain length ('m' parameter), the fluorosubstitution of the rigid core ('X_1' and 'X_2' parameters), the chiral chain length ('r' parameter) and the chiral centre structure ('r' and 's' parameters) have a significant impact on some physical properties, such as phase behaviour, crystallization/vitrification phenomena and crystallization kinetics.

For the 3FmX_1Ph$X_2$6.1 compounds with longer alkyl chains ('m' = 5, 7), the glass transition upon cooling and cold crystallization upon subsequent heating are usually observed. Shorter homologues with 'm' = 2-4 only crystallize. The vitrification of the smectic phases (SmC_A* or SmX_A*) occurs more often for the odd homologues. The fragility index of 3FmX_1Ph$X_2$6.1 is 72-129, so all compounds are fragile glass formers and their fragility does not depend on whether the vitrification occurs in the SmC_A* or SmX_A* phase. The kinetics of cold- and melt crystallizations exhibit different behaviour: (*i*) the non-isothermal cold crystallization is a complex phenomenon (for 3F5HPhH6.1 and 3F7FPhF6.1) or is controlled mainly by diffusion (for 3F7HPhF6.1), (*ii*) the isothermal cold crystallization is mainly driven by diffusion (for 3F7HPhH6.1, 3F5HPhH6.1, 3F6HPhF6.1, 3F7HPhF6.1 and 3F5FPhF6.1) and only for 3F7FPhH6.1 it is a complex process, (*iii*) the isothermal melt crystallization is a thermodynamic-controlled phenomenon for 3F5HPhH6.1, 3F5FPhF6.1 and 3F7FPhF6.1 or depends on diffusion for 3F7HPhH6.1 or is a complex process for 3F5FPhH6.1.

All 3FmHPhH7.1 compounds, elongated by two (-CH_2) groups, undergo glass transition, both those with a longer non-chiral alkyl chain ('m' = 5 vitrifies from the SmX_A* phase and 'm' = 7 vitrifies from the SmC_A* phase) and with shorter ones ('m' = 3 vitrifies from the CONDIS crystal phase). For 3F3HPhH7.1, the non-isothermal cold crystallization depends mainly on thermodynamic factor, while for 3F5HPhH7.1 and 3F7HPhH7.1 it is a complex process. For longer homologues ('m' = 5, 7), the isothermal cold crystallization is driven by diffusion, while the isothermal melt crystallization is controlled by thermodynamic factor. The glass transition temperature decreases as the

'm' parameter increases, proving a relation between the glass transition and the intramolecular chain motions.

The results obtained for 3FmX_1Ph$X_2$6.1 ('X_1', 'X_2' = H, F) show that the fluorinated compounds have lower transition temperatures than the samples which are not fluorosubstituted in the rigid core. The fluorination of the phenyl ring prevents the formation of the hexatic SmX_A* phase and significantly influences the glass forming properties of the compounds under study. The fluorosubstitution at the X_1 position leads to easier crystallization, while fluorosubstitution at the X_2 position increases the tendency to form the partially ordered smectic glass upon cooling. This is an exceptional type of glass, different from glasses obtained from the isotropic phase.

The length of the chiral chain ('r' parameter) has an impact on the temperatures of the phase transitions (temperatures are higher for compounds with a shorter chiral chain) and the temperature range of the SmC_A* phase occurrence (as the 'r' parameter increases, the range narrows). The 3F5HPhF6.1 ('r' = 6) crystallizes more efficiently than its shorter homologue, 3F5HPhF4.1 ('r' = 4). However, the opposite situation is observed for the 3F5HPhHr.1 and 3F7HPhHr.1 series, at which the fragility index is higher for longer homologues with 'r' = 7 than for compounds with 'r' = 6. It means that all molecular factors, e.g. the alkyl chain length and the fluorosubstitution of the phenyl ring should be taken into consideration, because they affect the behaviour of the 3FmX_1PhX_2r.1 compounds.

The chiral centre's structure also influences the glass transition, especially for 3F5HPhHr.s ('r.s' = 5.2 or 6.1). The 'r.s' = 5.2 isomer vitrifies from the SmC_A* phase upon slow and rapid cooling, while for 'r.s' = 6.1 sample the glass transition is observed from the SmX_A* phase only upon fast cooling. Likely, the varying lengths of the aliphatic chains connected to the chiral carbon atom could result in different patterns of the most energetically favourable molecular shapes for both similar molecules as the temperature shifts. Consequently, this diversity in how molecules are structured may impact how phases behave, which can be observed.

The results discovered could hold significant importance for upcoming investigations into LCs and their potential uses. Nevertheless, further research is needed to explore the relations between the mesophases' arrangement and crystallization/vitrification phenomena and its crystallization kinetics.

ACKNOWLEDGEMENTS

This work was financially supported by the National Science Centre (Grant MINIATURA 5: UMO-2021/05/X/ST3/00888). I thank Prof. E. Juszyńska-Gałązka for DSC measurements and data discussion, Prof. M. Jasiurkowska-Delaporte for BDS measurements and data discussion, Dr. A. Deptuch for resultts of 3FmX_1PhX_2r.1 (‘m’ = 2-7, ‘X_1’, ‘X_2’ = H, F, ‘r’ = 6) and 3F5HPhH5.2 compounds and data discussion, Dr. Ł. Kolek for results of 3F5HPhF4.1 compound, Prof. W. Zając for stimulating discussions and critical reading of the manuscript. I would also like to thank Prof. P. Kula and Prof. M. Urbańska for synthesizing the investigated materials.

REFERENCES

1 S. T. Lagerwall, A. Dahlgren, P. Jägemalm, P. Rudquist, K. D'havé, H. Pauwels, R. Dabrowski and W. Drzewinski, *Adv. Funct. Mater.*, 2001, **11**, 87–94.

2 K. D'havé, P. Rudquist, S. T. Lagerwall, H. Pauwels, W. Drzewinski and R. Dabrowski, *Appl. Phys. Lett.*, 2000, **76**, 3528–3530.

3 J. P. F. Lagerwall and F. Giesselmann, *ChemPhysChem*, 2006, **7**, 20–45.

4 J. P. F. Lagerwall and G. Scalia, *Curr. Appl. Phys.*, 2012, **12**, 1387–1412.

5 J. Wu, T. Usui and J. Hanna, *J. Mater. Chem.*, 2011, **21**, 8045.

6 J. A. Baird, B. Van Eerdenbrugh and L. S. Taylor, *J. Pharm. Sci.*, 2010, **99**, 3787–3806.

7 R. Brand, P. Lunkenheimer and A. Loidl, *J. Chem. Phys.*, 2002, **116**, 10386–10401.

8 N. Osiecka, E. Juszyńska-Gałązka, Z. Galewski, T. Jaworska-Gołąb, A. Deptuch and M. Massalska-Arodź, *J. Therm. Anal. Calorim.*, 2018, **133**, 961–967.

9 R. P. Marande and D. L. Uhrich, *Mol. Cryst. Liq. Cryst.*, 1986, **133**, 97–109.

10 A. García-Bernabé, R. Díaz Calleja, M. J. Sanchis, A. del Campo, A. Bello and E. Pérez, *Polymer (Guildf).*, 2004, **45**, 1533–1543.

11 Y. González, B. Palacios, M. A. Pérez Jubindo, M. R. de la Fuente and J. L. Serrano, *Phys. Rev. E*, 1995, **52**, R5764–R5767.

12 Ł. Kolek, M. Jasiurkowska-Delaporte and E. Juszyńska-Gałązka, *J. Mol. Liq.*, 2021, **323**, 115040.

13 Ł. Kolek, M. Massalska-Arodź, K. Adrjanowicz, T. Rozwadowski, K. Dychtoń, M. Drajewicz and P. Kula, *J. Mol. Liq.*, 2020, **297**, 1–8.

14 S. H. Chen, *J. Soc. Inf. Disp.*, 2004, **12**, 205.

15 A. Drzewicz, E. Juszyńska-Gałązka, W. Zając, M. Piwowarczyk and W. Drzewiński, *J. Mol. Liq.*, 2020, **319**, 114153/1–12.

16 T. Rozwadowski, M. Massalska-Arodź, Ł. Kolek, K. Grzybowska, A. Bąk and K. Chłędowska, *Cryst. Growth Des.*, 2015, **15**, 2891–2900.

17 T. Ishikawa, A. Honda and K. Miyamura, *CrystEngComm*, 2022, **24**, 5900–5906.

18 M. Paluch, J. Knapik, Z. Wojnarowska, A. Grzybowski and K. L. Ngai, *Phys. Rev. Lett.*, 2016, **116**, 025702.

19 M. Żurowska, R. Dąbrowski, J. Dziaduszek, K. Garbat, M. Filipowicz, M. Tykarska, W. Rejmer, K. Czupryński, A. Spadło, N. Bennis and J. M. Otón, *J. Mater. Chem.*, 2011, **21**, 2144–2153.

20 A. Deptuch, A. Lelito, E. Juszyńska-Gałązka, M. Jasiurkowska-Delaporte and M. Urbańska, *Phys. Chem. Chem. Phys.*, 2023, **25**, 12379–12393.

21 A. Deptuch, S. Lalik, M. Jasiurkowska-Delaporte, E. Juszyńska-Gałązka, A. Drzewicz, M. Urbańska and M. Marzec, *Phys. Rev. E*, 2022, **105**, 024705.

22 S. Ciastek, K. Szymańska, P. Kaszyński, M. Jasiński and D. Pociecha, *Liq. Cryst.*, 2018, **45**, 11–21.

23 J. Herman, A. Aptacy, E. Dmochowska, P. Perkowski and P. Kula, *Liq. Cryst.*, 2020, **47**, 2332–2340.

24 M. Pytlarczyk, J. Herman, P. Harmata, S. Urban and P. Kula, *Liq. Cryst.*, 2018, **45**, 1460–1469.

25 P. Perkowski, Z. Raszewski, W. Piecek, K. Ogrodnik, M. Żurowska, R. Dąbrowski and X. W. Sun, *Mol. Cryst. Liq. Cryst.*, 2009, **509**, 328/[1070]-335/[1077].

26 M. Tykarska, A. Drzewicz, M. Szala and M. Żurowska, *Liq. Cryst.*, 2018, **45**, 1385–1395.

27 A. Drzewicz, A. Bombalska and M. Tykarska, *Liq. Cryst.*, 2019, **46**, 754–771.

28 M. Tykarska, M. Czerwiński and A. Drzewicz, *J. Mol. Liq.*, 2019, **292**, 110379/1–13.

29 A. Deptuch, N. Górska, M. Srebro-Hooper, J. Hooper, M. Dziurka and M. Urbańska, *Chem. Phys.*, 2023, **573**, 111977.

30 A. Deptuch, T. Jaworska-Gołąb, M. Dziurka, J. Hooper, M. Srebro-Hooper, M. Urbańska, M. Tykarska and M. Marzec, *Phys. Rev. E*, 2023, **107**, 034703.

31 M. Żurowska, R. Dąbrowski, J. Dziaduszek, K. Czupryński, K. Skrzypek and M. Filipowicz, *Mol. Cryst. Liq. Cryst.*, 2008, **495**, 145/[497]-157/[509].
32 K. Milewska, W. Drzewiński, M. Czerwiński and R. Dąbrowski, *Liq. Cryst.*, 2015, **42**, 1–11.
33 M. Żurowska, M. Filipowicz, M. Czerwiński and M. Szala, *Liq. Cryst.*, 2019, **46**, 299–308.
34 S. Havriliak and S. Negami, *Polymer (Guildf).*, 1967, **8**, 161–210.
35 M. D. Ediger, C. A. Angell and S. R. Nagel, *J. Phys. Chem.*, 1996, **100**, 13200–13212.
36 R. Böhmer, K. L. Ngai, C. A. Angell and D. J. Plazek, *J. Chem. Phys.*, 1993, **99**, 4201–4209.
37 M. D. Ediger, P. Harrowell and L. Yu, *J. Chem. Phys.*, 2008, **128**, 034709.
38 A. Sanz and K. Niss, *Cryst. Growth Des.*, 2017, **17**, 4628–4636.
39 D. W. Henderson, *J. Non. Cryst. Solids*, 1979, **30**, 301–315.
40 T. Ozawa, *Polymer (Guildf).*, 1971, **12**, 150–158.
41 H. E. Kissinger, *J. Res. Natl. Bur. Stand. (1934).*, 1956, **57**, 217.
42 J. A. Augis and J. E. Bennett, *J. Therm. Anal.*, 1978, **13**, 283–292.
43 D. Georgopoulos, S. Kripotou, E. Argyraki, A. Kyritsis and P. Pissis, *Mol. Cryst. Liq. Cryst.*, 2015, **611**, 197–207.
44 S. Napolitano and M. Wübbenhorst, *Macromolecules*, 2006, **39**, 5967–5970.
45 M. Avrami, *J. Chem. Phys.*, 1939, **7**, 1103–1112.
46 A. Mishra, R. Dabrowski and R. Dhar, *J. Mol. Liq.*, 2018, **249**, 106–109.
47 V. Novotná, M. Kašpar, V. Hamplová, M. Glogarová, I. Rychetský and D. Pociecha, *Liq. Cryst.*, 2004, **31**, 1131–1141.
48 A. Deptuch, M. Piwowarczyk, M. Jasiurkowska-Delaporte, J. Kim, M. Urbańska, M. Skolarczyk, T. Jaworska-Gołąb and M. Marzec, *Crystals*, 2022, **12**, 1028.
49 A. Deptuch, M. Jasiurkowska-Delaporte, W. Zając, E. Juszyńska-Gałązka, A. Drzewicz and M. Urbańska, *Phys. Chem. Chem. Phys.*, 2021, **23**, 19795–19810.
50 A. Deptuch, E. Juszyńska-Gałązka, A. Drzewicz and M. Urbańska, *J. Cryst. Growth*, 2022, **593**, 126771.
51 A. Deptuch, M. Jasiurkowska-Delaporte, E. Juszyńska-Gałązka, A. Drzewicz and M. Urbańska, *Crystals*, 2022, **12**, 1583.
52 A. Deptuch, M. Marzec, T. Jaworska-Gołąb, M. Dziurka, J. Hooper, M. Srebro-Hooper, P. Fryń, J. Fitas, M. Urbańska and M. Tykarska, *Liq. Cryst.*, 2019, **46**, 2201–2212.
53 A. Deptuch, M. Jasiurkowska-Delaporte, M. Urbańska and S. Baran, *J. Mol. Liq.*, 2022, **368**, 120612.
54 A. Deptuch, T. Jaworska-Gołąb, M. Marzec, D. Pociecha, J. Fitas, M. Żurowska, M. Tykarska and J. Hooper, *Phase Transitions*, 2018, **91**, 186–198.
55 A. Deptuch, T. Jaworska-Gołąb, M. Marzec, M. Urbańska and M. Tykarska, *Phase Transitions*, 2019, **92**, 126–134.
56 A. Deptuch, E. Juszyńska-Gałązka, A. Drzewicz, M. Piwowarczyk, M. Urbańska and M. Tykarska, *Phase Transitions*, 2023, **96**, 149–156.
57 A. Deptuch, M. Jasiurkowska-Delaporte, E. Juszyńska-Gałązka, A. Drzewicz, M. Piwowarczyk, M. Urbańska and S. Baran, *J. Phys. Chem. B*, 2022, **126**, 6547–6561.
58 A. Deptuch, M. Jasiurkowska-Delaporte, E. Juszyńska-Gałązka, A. Drzewicz, W. Zając and M. Urbańska, *Crystals*, 2021, **11**, 1487/1–19.
59 S. Lalik, A. Deptuch, P. Fryń, T. Jaworska–Gołąb, D. Dardas, D. Pociecha, M. Urbańska, M. Tykarska and M. Marzec, *Liq. Cryst.*, 2019, **46**, 2256–2268.
60 A. Deptuch, E. Juszyńska-Gałązka, M. Jasiurkowska-Delaporte, A. Drzewicz, M. Piwowarczyk and M. Urbańska, *Phase Transitions*, 2023, **96**, 166–185.
61 A. Deptuch, A. Drzewicz, M. Dziurka, N. Górska, J. Hooper, T. Jaworska-Gołąb, E. Juszyńska-Gałązka, M. Marzec, M. Piwowarczyk, M. Srebro-Hooper, M. Tykarska and M. Urbańska, *Mater. Res. Bull.*, 2022, **150**, 111756/1–11.
62 A. Deptuch, M. Jasiurkowska-Delaporte, E. Juszyńska-Gałązka, A. Drzewicz, W. Zając and M. Urbańska, *Crystals*, 2022, **12**, 1588.
63 R. Böhmer, K. L. Ngai, C. A. Angell and D. J. Plazek, *J. Chem. Phys.*, 1993, **99**, 4201–4209.

64 A. Deptuch, A. Lelito and M. Urbańska, *Acta Phys. Pol. A*, 2023, **144**, 93–98.
65 A. Deptuch, E. Juszyńska-Gałązka, M. Jasiurkowska-Delaporte, A. Drzewicz, M. Piwowarczyk and M. Urbańska, *Phase Transitions*, 2023, **96**, 166–185.
66 A. Drzewicz, E. Juszyńska-Gałązka, A. Deptuch and P. Kula, *Crystals*, 2022, **12**, 1401.
67 A. Drzewicz, M. Jasiurkowska-Delaporte, E. Juszyńska-Gałązka, M. Gałązka, W. Zając and P. Kula, *Phys. Chem. Chem. Phys.*, 2021, **23**, 17466–17478.
68 A. Drozd-Rzoska, S. J. Rzoska and K. Czupryński, *Phys. Rev. E*, 2000, **61**, 5355–5360.
69 A. Drzewicz, M. Jasiurkowska-Delaporte, E. Juszyńska-Gałązka, W. Zając and P. Kula, *Phys. Chem. Chem. Phys.*, 2021, **23**, 8673–8688.
70 A. Drzewicz, M. Jasiurkowska-Delaporte, E. Juszyńska-Gałązka, A. Deptuch, M. Gałązka, W. Zając and W. Drzewiński, *Phys. Chem. Chem. Phys.*, 2022, **24**, 4595–4612.
71 A. Drzewicz, E. Juszyńska-Gałązka, M. Jasiurkowska-Delaporte and P. Kula, *CrystEngComm*, 2022, **24**, 3074–3087.
72 A. Drzewicz, E. Juszyńska-Gałązka, W. Zając and P. Kula, *Crystals*, 2020, **10**, 655/1–21.
73 R. Xie, A. R. Weisen, Y. Lee, M. A. Aplan, A. M. Fenton, A. E. Masucci, F. Kempe, M. Sommer, C. W. Pester, R. H. Colby and E. D. Gomez, *Nat. Commun.*, 2020, **11**, 893.
74 A. D. L. Chandani, Y. Ouchi, H. Takezoe, A. Fukuda, K. Terashima, K. Furukawa and A. Kishi, *Jpn. J. Appl. Phys.*, 1989, **28**, L1261.
75 Ł. Kolek, M. Massalska-Arodź, D. Majda, B. Wantusiak, S. Zalewski and P. Kula, *Acta Phys. Pol. A*, 2012, **122**, 370–374.
76 Ł. Kolek, M. Massalska-Arodź, M. Paluch, K. Adrjanowicz, T. Rozwadowski and D. Majda, *Liq. Cryst.*, 2013, **40**, 1082–1088.
77 Ł. Kolek, M. Massalska-Arodź, D. Majda, B. Suchodolska and S. Zalewski, *Acta Phys. Pol. A*, 2013, **124**, 909–912.
78 Ł. Kolek, M. Jasiurkowska-Delaporte, M. Massalska-Arodź, W. Szaj and T. Rozwadowski, *J. Mol. Liq.*, 2020, **320**, 114338.
79 Ł. Kolek, M. Jasiurkowska-Delaporte, E. Juszyńska-Gałązka and T. Rozwadowski, *J. Mol. Liq.*, 2021, **339**, 117076.
80 M. Jasiurkowska-Delaporte, T. Rozwadowski, E. Dmochowska, E. Juszyńska-Gałązka, P. Kula and M. Massalska-Arodź, *J. Phys. Chem. B*, 2018, **122**, 10627–10636.
81 H. Tanaka, *J. Non. Cryst. Solids*, 2005, **351**, 678–690.